Univerzita Karlova v Praze
Matematicko-fyzikální fakulta

Diplomová práce

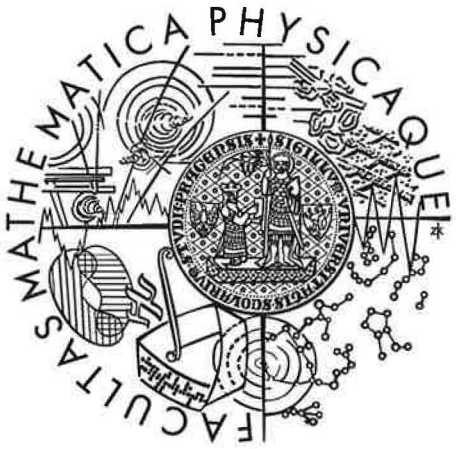

Tomáš Kráľ

Studie parametrizace fyzikálních účinků nerozlišené orografie v numerickém předpovědním modelu s použitím situace větrné bouře v Tatrách 19/11/2004

Katedra meteorologie a ochrany prostředí
Vedoucí diplomové práce: Prof. RNDr. Jan Bednář, CSc.
Studijní program: Fyzika - Meteorologie a klimatologie

Na tomto mieste by som sa chcel poďakovať RNDr. Radmile Brožkovej, CSc. za technickú podporu, odborné rady a usmerňovanie pri vypracovaní diplomovej práce a Jean-François Geleynovi za množstvo cenných nápadov, inšpiráciu a všetok venovaný čas. Ďalej ďakujem svojmu školitelovi Prof. RNDr. Janovi Bednářovi, CSc. a samozrejme nemôžem vynechať poďakovanie Českému hydrometeorologickému ústavu za to, že mi umožnil pracovať na diplomovej práci v profesionálnom prostredí oddelenia numerickej predpovede počasia.

Prohlašuji, že jsem svou diplomovou práci napsal samostatně a výhradně s použitím citovaných pramenů. Souhlasím se zapůjčováním práce.

V Praze *11.4.2007* *Tomáš Král'*

Contents

Název práce: *Studie parametrizace fyzikálních účinků nerozlišené orografie v numerickém předpovědním modelu s použitím situace větrné bouře v Tatrách 19/11/2004*
Autor: *Tomáš Král'*
Katedra: *Katedra meteorologie a ochrany prostředí*
Vedoucí diplomové práce: *Prof. RNDr. Jan Bednář, CSc.*
E-mail vedoucího: *Jan.Bednar@ruk.cuni.cz*

Abstrakt:

Situace větrné bouře v Tatrách z 19/11/2004 je velice vhodná pro porozumnění a vyladění schémat parametrizace účinků té části orografie, která není modelem rozlišena. Jednak proto, že tato synoptická situace je téměř nezávislá na třecím efektu mezní vrstvy; jde totiž o jednu z vyjimečných bouří která v plné síle pronikla hluboko nad kontinent. Jednak také proto, že tato synoptická situace byla velmi dobře předpovězena modelem ALADIN a je dostatečně zdokumentována, což vytváří dobré podmínky pro navrženou studii.

Tento případ je ještě zajímavější tím, že náhrada účinů tzv. obálkové orografie novým a realističtějším schématem parametrizace nerozlišené orografie vedla k méně dobré simulaci proudění vzduchu přes hřeben Tater; tento výsledek může stejně tak dobře být důsledkem toho, že základní předpověď byla lepší z důvodu vzájemně se kompenzujících chyb, anebo také proto, že v současné parametrizaci chybí zachycení některého procesu. V kadém případě je však tato situace výhodná v tom, že by měla jít zreprodukovat v semi-akademickém prostředí s izolovanou horskou překážkou a zjednodušenou atmosférou s hyper-baroklinním vývojem. To jistě povede k lepšímu porozumnění odezvy současné parametrizace a v optimistickém případě k návrhu takové její modifikace, která by zlepšila předpověď větrné bouře v Tatrách a zároveň by v průměru neměla dopad na kvalitu simulací méně extrémních případů.

Klíčová slova: *parametrizace, dopřední odpor, zdvih, obálková orografie*

Title: *Study of parametrisation of physical effects of unresolved orography in numerical prediction model with use of situation of wind storm in Tatras 19/11/2004*
Author: *Tomás Král'*
Department: *Department of meteorology and environment protection*
Supervisor: *Prof. RNDr. Jan Bednář, CSc.*
Supervisor's e-mail address: *Jan.Bednar@ruk.cuni.cz*

Abstract:

Situation of downslope windstorm in Tatras on 19/11/2004 represents an appropriate conditions for better understanding and tuning of parametrisation schemes of sub-grid scale orography effects. One of the reasons is that the synoptical situation is almost independent of the friction effect in boundary layer; as it is the one of the rare severe windstorms, that reached the interior of the continent with a remarkable strength. Another reason is that this synoptical situation was successfully forecasted by NWP model ALADIN and is well documented which creates favourable conditions for further research.

More importantly, this case is interesting because the substitution of the effects of envelope orography by a new and more sophisticated parametrisation scheme was not so successful in forecasting of this extreme event which can be the result of the fact that the reference forecast was better because of some compensating errors, or alternatively, because present parametrisation lacks a representation of some missing effects. Nevertheless, this situation could be reproduced in semi-academical environment with isolated mountain obstacle and simplified atmospheric conditions with hyper-baroclinic evolution. This should lead to a better understanding of the response of present parametrisation and more optimistically, to a proposal of some modifications that would improve the forecast of the Tatra case and at the same time, that would not negatively affect the overall quality of the forecast of less severe events.

Keywords: *parametrisation, form-drag, lift, envelope*

Introduction

It is well known that unresolved orography can significantly influence the dynamics of the atmosphere through many complex sub-grid interactions. For instance, it forces gravity waves that can propagate up to the stratosphere and exert drag on the mean flow in the process of turbulent dissipation. At low levels, sub-grid mountains generate additional drag on large scale flow through non-linear processes, e.g. upstream flow blocking, low level wave breaking. Furthermore, sub-grid orography can also contribute to the steady planetary waves through the mechanism of potential vorticity conservation in the process of vortex compression in the vicinity of the mountains. Thus it is generally agreed that representation of sub-grid scale orography effects is crucial for further improvement of numerical weather prediction (NWP). However, the resolution of nowadays operational NWP models is still not sufficient to explicitly resolve these processes and thus they are parametrized by various means. The one of the first successfully used concepts (apart from other orography enhancing techniques) was envelope orography. However, the recent boom in data assimilation and new and more sophisticated parametrisations made the concept to fade almost everywhere. New schemes of parametrisation of sub-grid scale orography effects usually include representation of the gravity wave drag, form drag (as a substitute for the flow blocking) and lift effect. Although the necessity of sub-grid scale orography effects parametrization will probably fade out in the future, as the NWP models are constantly progressing towards higher resolutions, they will be still needed at least in global NWP models for the time being.

Despite many efforts, a transition from envelope to mean orography in NWP model ALADIN can still not be considered as fully solved. The main objectives of the work presented here are to develop complementing diagnostic tools and invent appropriate methodology for verification and tuning of sub-grid scale orography drag parametrization in ALADIN/ARPEGE numerical model with the aim to better understand the overall response of the scheme. The goal is to test the latest proposals and implement a new modifications that would lead to a compensation for the dramatic impact of the suppression of the envelope orography.

In the first chapter, an introduction to the linear theory of internal gravity waves is presented to give a better insight to the basic principles and concepts the wave-drag part of parametrization is based on. Next chapter provides more detailed description of the present ALADIN/ARPEGE scheme as the understanding of its particular elements is substantial for the further development. Additionally, we will also touch the concept of envelope orography, owing to the fact that the target of this work is to obtain its equivalent counterpart effect improving the current parametrisation scheme. The last chapter deals with detailed analysis of the impacts of envelope orography removal to reveal the weaknesses of current GWD scheme and better understand which effects are insufficiently represented. In the further, we propose

a new tuning as one of the possible solutions and we also test several new ideas giving their theoretical justification as well as the validation of obtained results.

Chapter 1

Theoretical description

1.1 Linear internal gravity waves

In order to prepare for a description of gravity-wave drag parametrization, we discuss in this section some properties of internal gravity waves excited by orography. Consider a case of two-dimensional, inviscid and incompressible stratified flow over an obstacle where the mean state is given by the wind profile $U(z)$ and by a density distribution $\rho_0(z)$. We will be exclusively concerned with a stationary response of air-flow to forcing by mountains and we will neglect any transient responses. The steady state assumption implies that local time derivatives will vanish. We will further consider only such wavelengths that effect of the Earth's rotation can be ignored. After a scale analysis for a typical wind speeds of order 10 m/s this restricts our discussion to wavelengths less than 10 km. In the following, we shall use the *Boussinesq approximation* whereby density is treated as a constant except where it is coupled with gravity, i.e. buoyancy term (see Holton, 1992). Then disturbances in the flow are controlled by the following linearized set of equations:

$$U\frac{\partial u'}{\partial x} + w\frac{\partial U}{\partial z} + \frac{1}{\rho_m}\frac{\partial p'}{\partial x} = 0 \tag{1.1}$$

$$U\frac{\partial w'}{\partial x} + \frac{1}{\rho_m}\frac{\partial p'}{\partial z} + \frac{\rho'}{\rho_0}g = 0 \tag{1.2}$$

$$\frac{\partial u'}{\partial x} + \frac{\partial w'}{\partial z} = 0 \tag{1.3}$$

$$U\frac{\partial \theta'}{\partial x} + w'\frac{\partial \theta_0}{\partial z} = 0. \tag{1.4}$$

where u', w', p' and ρ' are respectively velocity, pressure and density perturbations of mean values. The system of four equations above can be reduced after some straightforward manipulations to one equation of the form

$$\frac{\partial^2 w'}{\partial z^2} + \frac{\partial^2 w'}{\partial x^2} - \left[\frac{1}{U}\frac{\partial^2 U}{\partial z^2} + \frac{N^2}{U^2}\right]w' = 0 \tag{1.5}$$

with

$$N^2 = \frac{g}{\theta_0}\frac{\partial \theta_0}{\partial z} \tag{1.6}$$

the square of Brunt-Väisäla frequency. For simplicity, we assume the solution in a form of a single Fourier harmonic

$$w'(x,z) = \hat{w}(k,z)\, e^{i(kx)} \tag{1.7}$$

which is appropriate for imposed sinusoidal lower boundary condition

$$h(x) = h_0\, e^{ikx}. \tag{1.8}$$

The solution (1.7) represents linear internal gravity wave with zero phase speed and horizontal wavenumber k. Of course, it is understood that we take only the real part as a physical solution. If we substitute (1.7) to (1.5) we will yield the *Taylor-Goldstein* equation

$$\frac{\mathrm{d}\hat{w}}{\mathrm{d}z^2} + \left[\ell^2 - k^2\right]\hat{w} = 0 \tag{1.9}$$

where ℓ is the *Scorer parameter*

$$\ell^2 = \frac{N^2}{U^2} - \frac{U''}{U}. \tag{1.10}$$

Double primes over U in (1.10) denote the second derivative of U with respect to z. From definition of ℓ one can easily see that stratification with concave wind profile ($U'' < 0$) presents favorable conditions for vertically propagating mode, but this fact does not mean it is necessary condition. Indeed, for a typical atmospheric conditions, the second term in (1.10) is one order smaller then the first one which is usually dominant with its typical values of order $10^{-6}m^{-1}$. However, second term might not be neglected when

$$\frac{(U''/U)}{(N^2/U^2)} \sim 1.$$

For simplicity, we will further assume constant profile of basic state velocity U, so that second term in (1.10) can be ignored. A glance at the differential equation (1.9) shows that character of solution depends on whether

$$\ell^2 > k^2 \qquad \text{or} \qquad \ell^2 < k^2.$$

In the former case, the solution will be oscillatory in z, while in the latter case it will be exponentially decaying with height. Physical interpretation of change in the solution can be done for a simple case of constant U. In this case, $\ell^2 = N^2/U^2$. If we put ourselves in a frame moving to the right with basic flow, fluid appears to be at rest but is disturbed by lower boundary (with wave number k) moving to the left at speed U forcing a response of frequency Uk. If that frequency is greater than buoyancy frequency N, we clearly can not have a wavelike response in z. One should note that condition $Uk > N$ is simply $\ell^2 < k^2$.

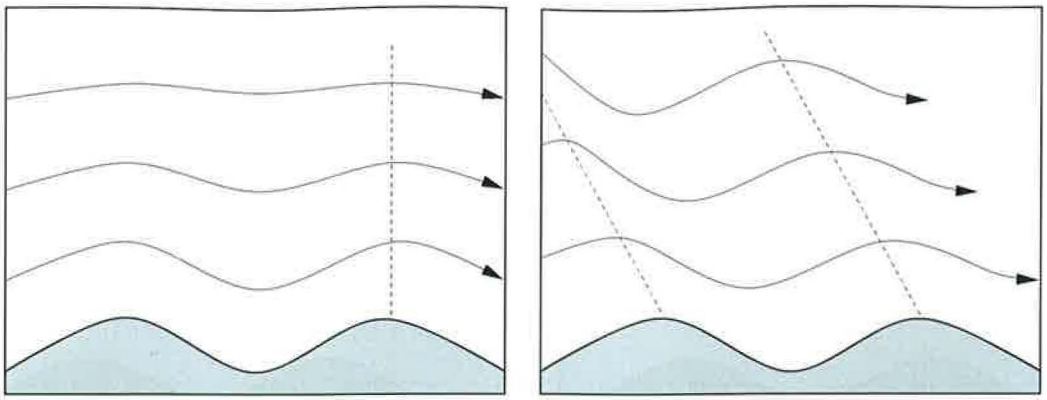

(a) (b)

Figure 1.1: Streamlines over wavy orography for (a) vertically decaying and (b) vertically propagating waves with slant in phase lines

Let us first examine the case where $\ell^2 < k^2$. In this case, the solution for $\hat{w}$ is

$$\hat{w}(z) = Ae^{-mz} + Be^{mz} \tag{1.11}$$

with

$$m^2 = k^2 - \ell^2 > 0.$$

We want the solution to remain bounded when $z \to \infty$. This clearly requires that we choose $B = 0$. Remaining constant is determined by lower boundary condition

$$\begin{aligned} w'(z=0) &= U\frac{\partial h}{\partial x} \\ &= ikUh_0 e^{ikx} \end{aligned} \tag{1.12}$$

giving

$$A = ikUh_0. \tag{1.13}$$

Thus the vertical velocity distribution is out of phase with topography (rising motion at the upstream face and sinking at the downstream face) and diminishes exponentially with height. In this parameter regime no internal gravity waves can be excited.

Now, let's consider more interesting case when $\ell^2 > k^2$. Here we define

$$m^2 = \ell^2 - k^2 > 0,$$

so that the solution for amplitude of vertical velocity perturbation is

$$\hat{w}(z) = Ae^{imz} + Be^{-imz}. \tag{1.14}$$

However, the former condition that the solution is finite for large positive z does not help at all in rejecting either the A or B solution of $\hat{w}$. So with lower boundary condition we have only one equation for the two unknowns, A and B. We can solve this physically incomplete

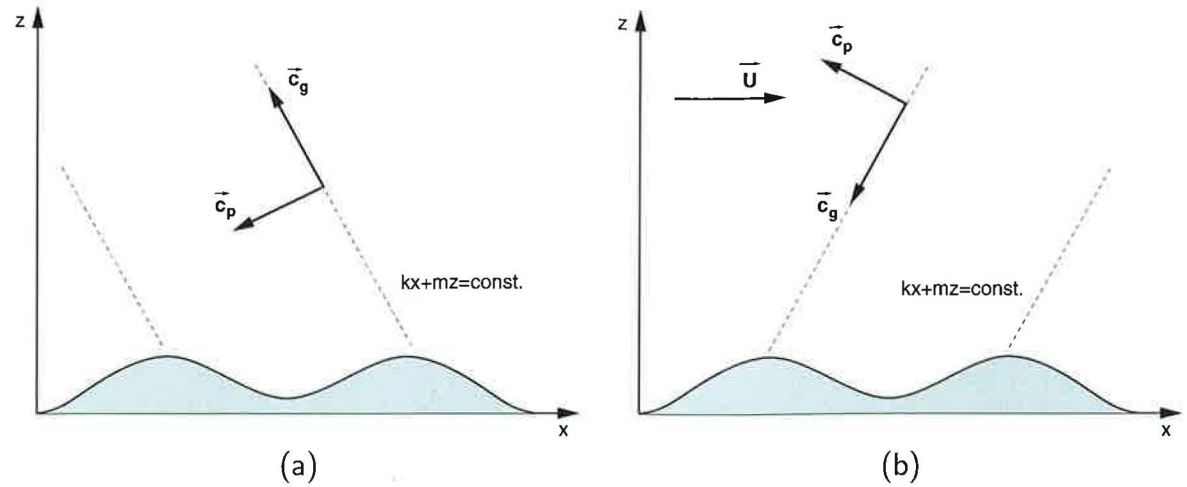

Figure 1.2: Group and phase velocity vectors relative to the mean flow for (a) phase lines tilting upstream (A solution) and (b) phase lines tilting downstream (B solution).

problem by implying *radiation condition*. Simply put, it states that we have to decide on the direction of energy radiation. Since energy source is situated on the ground, it is clear that in our framework, the radiation will be outgoing, that is, the energy flux in z-direction is positive. With the above solution for $\hat{w}$ we have

$$w'(x,z) = Ae^{i(kx+mz)} + Be^{i(kx-mz)}. \tag{1.15}$$

The part of solution with coefficient A has phase lines tilting upstream, while the B solution has phase lines tilting downstream (for $U > 0$). In next, we will use a remarkable property of internal gravity waves that group velocity and phase propagation are actually oriented perpendicular to each other in a vertical plane, and more interestingly, the vertical component of group velocity has opposite sign to that of vertical component of phase speed relative to the mean flow. We can see in Fig. 1.2 that correct solution, satisfying upward energy flux, would be the one with coefficient A, while B solution represents incoming radiation from infinity which is not consistent with our physical description.

Stable stratification, wide ridges, and comparatively weak zonal flow thus provide favorable conditions for formation of vertically propagating orographic waves. For a simple case of constant U we can get an estimate of wavelengths that are connected with vertically propagating solution. In this case $\ell^2 = N^2/U^2$. If we look for a solution that is wave-like in the vertical then

$$\lambda = \frac{2\pi}{k} > \frac{2\pi U}{N}. \tag{1.16}$$

As we will see later, it is the wave-like modes with wavelengths greater than $2\pi U/N$ that are associated with orographic drag. In typical conditions with $U \sim 10\ m/s$ and $N \sim 10^{-2}\ s^{-1}$ the critical wavelength is few kilometers and is therefore not properly resolved by numerical weather prediction models.

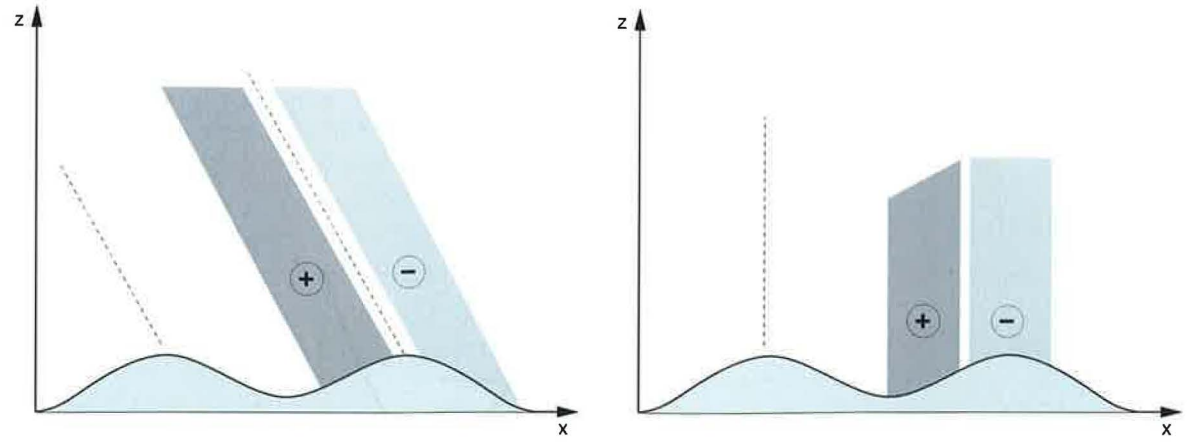

(a) (b)

Figure 1.3: Schematic representation of perturbation pressure field for (a) vertically propagating waves and (b) decaying waves.

1.2 Gravity wave stress

Generally, stress is a force per unit horizontal area exerted on the atmosphere. Here we are concerned primarily with orographic stress caused by generation of internal gravity waves. In Fig. 1.1 one can see the wavelike pattern of streamlines generated by the orography. The slope of lines of constant phase is a direct cause of the force to orography. The essential mechanism of gravity wave drag may be illustrated by using the Bernoulli equation for an incompressible flow (a good enough approximation)

$$\frac{U^2}{2} + \frac{p}{\rho_0} + gz = \text{constant on streamlines.} \tag{1.17}$$

As one can see, regions of high velocity will be associated with low pressure and vice versa, hence generating a disturbance p' in the pressure field. Let us examine perturbation pressure field in two particular cases discussed in the previous section. From (1.4) one can easily find

$$\frac{\partial p'}{\partial x} = \rho_0 U \frac{\partial w'}{\partial z}. \tag{1.18}$$

For the first case of vertically decaying waves with solution (1.11) one can find that pressure field is in phase with the topography, thus being symmetrical about the ridge with the lowest pressure anomaly over the ridge crest (see Fig. 1.3). Clearly, in this parameter regime there is no net force on the topography. The absence of drag is not too surprising because if Uk is much greater than N, the fluid will respond as if the stratification were zero and the resulting pressure field corresponds to the ventury effect. Now we consider a second case when $Uk < N$ so that internal gravity waves are generated. Here, on the contrary, perturbation pressure field is $\frac{\pi}{2}$ out of phase with topography. High pressure occurs on the upstream face of each ridge while the downstream face has low pressure. This leads to the net force on the topography, or equivalently to the force of orography to the atmosphere. As a final remark, we shall now see that existence of wave drag is directly related to the ability of the flow to support vertically propagating waves.

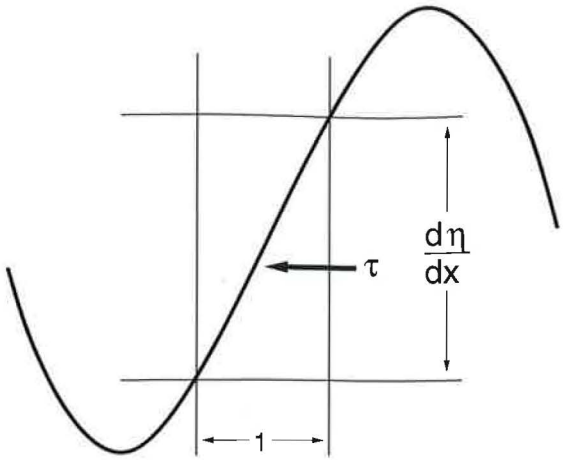

Figure 1.4: Horizontal pressure force on the wave surface.

A horizontal pressure force on a material surface deformed by gravity wave is illustrated in Fig. 1.4. The horizontal force per unit area averaged over a wavelength can be expressed as

$$\overline{\tau} = \overline{p' \frac{\partial \eta}{\partial x}}. \tag{1.19}$$

In our framework, vertical displacement can be defined as

$$w' = \frac{\mathrm{d}\eta}{\mathrm{d}t} = U \frac{\partial \eta}{\partial x} \tag{1.20}$$

and from (1.4) one finds

$$p' = -\rho_0 U u' \tag{1.21}$$

which gives together

$$\overline{\tau} = -\rho_0 \overline{u'w'}. \tag{1.22}$$

To determine the total force acting on a layer of fluid between two surfaces, one must consider both the force at the top $\overline{\tau} + \delta\overline{\tau}$ and force at the bottom $\overline{\tau}$. If we assume a layer of thickness δz, the total average force then becomes

$$\overline{\tau} + \delta\overline{\tau} - \overline{\tau} = \delta\overline{\tau} = \frac{\partial \overline{\tau}}{\partial z}\delta z = -\frac{\partial}{\partial z}(\rho_0 \overline{u'w'})\delta z \tag{1.23}$$

where $\rho_0 \overline{u'w'}$ is wave-induced vertical flux of horizontal momentum. The mass of unit horizontal area is $\rho_0 \delta z$ so the u-momentum equation for the layer of fluid is

$$\rho_0 \frac{\partial U}{\partial t} = -\frac{\partial}{\partial z}(\rho_0 \overline{u'w'}). \tag{1.24}$$

Hence we see that resultant force is non-zero when $\rho_0 \overline{u'w'}$ changes with height. This equation can be used to consistently calculate the small, second order changes in the mean flow due to waves. Gravity wave drag parametrization, that will be discussed in the next chapter, is fundamentally concerned with representing the change of vertical flux of horizontal momentum with height.

1.3 Generalisation

One should realise that results of previous section were obtained for restrictive conditions of constant base state and purely sinusoidal lower boundary condition. In reality, both wind U and stability N vary considerably with height and moreover, ridges are usually isolated rather than periodic. Thus a variety of responses are possible depending on shape of the mountain and wind and stability profiles. Terrain of general shape can be approximated by the Fourier superposition of modes

$$H(x) = \int_{-\infty}^{\infty} H_l \, exp(ik_l x) \, \mathrm{d}l. \tag{1.25}$$

We can then express the solution to the equation (1.5) in the form

$$w'(x,z) = \int_{-\infty}^{\infty} W_l \, exp[i(k_l x + m_l z)] \, \mathrm{d}l. \tag{1.26}$$

We can see that flow over a ridge of general shape generates whole spectrum of waves where individual Fourier modes will yield vertically propagating or decaying contribution to the total solution. Narrow ridges will produce dominantly short wavenumber waves decaying with hight and vice versa. Closer discussion is beyond the scope of this work. In gravity wave drag parametrisation, we are primarily concerned in final quantitative effect of internal gravity waves on the basic zonal flow rather then precise description of particular wave pattern.

Chapter 2

Mountain drag parametrisation

2.1 Introduction

The parametrisation of subgrid scale orographic effects has had a significant positive impact to the gradually increasing quality of the NWP forecasts. Representation of unresolved orographic features is one of the most difficult problems in meteorological modeling. The route from simple enhanced orographic techniques to present sophisticated parametrisations required a lot of scientific development because of the large variety of processes involved. Orography can significantly modify the flow generating broad spectrum of waves, inducing blocking effect and additional turbulence. Besides, it presents an elevated heat source and influences distribution and intensity of rainfall. In this Section, we will be primarily concerned by the impact of the unresolved orography on the flow. However, it does not exclude a possibility that we can indirectly influence also other quantities because of a complex system of various feedbacks that are present in the atmosphere.

Generally, the total drag exerted by the orography can be categorized following the diagram in Fig. 2.1. As can be seen at the top of the picture, the total drag is divided into two fundamentally different components: friction drag and pressure drag. The friction drag is the part of the resistance due to molecular viscosity of the air which is however extremely small

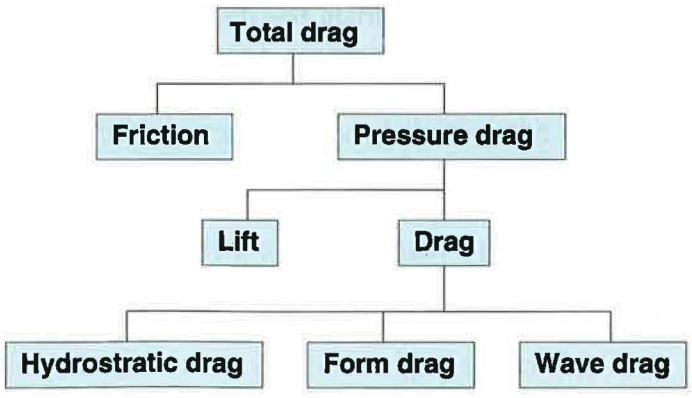

Figure 2.1: Schematic categorisation of different contributions to the total drag.

compared to the latter one. The pressure drag is divided in two parts one of which is parallel to the flow - drag, and the other is orthogonal to the flow - lift. The lift effect exists mainly due to the Coriolis force however, obstacles with high asymmetry can induce large lift effect, too. The parallel drag is further divided in three parts: (i) the hydrostatic drag, which would exist even if there is no flow motion because it is generated by the pressure differences between two sides of a mountain, (ii) the form drag, which is directly related to the pressure differences at the windward and lee side of the obstacle locally decelerating the flow, (iii) wave drag, which is related to the deposition of the waves that are generated by the obstacles. In this case, associated deceleration is not necessarily local and can happen at some distances (horizontal and vertical from obstacle).

There are generally four ways how one can represent the subgrid scale effects of unresolved orography:

- an effective surface roughness length
- an additional artificial increase of model orography (envelope orography)
- a parametrisation of subgrid orography stress
- a lift effect

Here, we shall primarily deal with last three ones, though we will marginally touch also the first one. All these four methods exist in ALADIN/ARPEGE framework and can be used at the same time, altho it is not mandatory. In the next Sections we will discuss the last three methods in more detail starting with envelope orography followed by description of ALADIN/ARPEGE GWD scheme including the latest modifications (Geleyn et al., 2005).

2.2 Envelope orography

In the beginning of 80's a step to the higher resolution of NWP models brought some deterioration of the mean westerly flow at moderate latitudes, especially above Northern Hemisphere continents during wintertime and at the same time GCMs experienced problems in representation of stationary planetary waves which was attributed mainly to an insufficient representation of orography. The concept of envelope orography was firstly introduced by Wallace et al. (1983) with the aim to propose a solution to the above mentioned problems. This was one of many enhanced orography techniques that were following the work of Pierrehumbert (1983) who showed that under linear theory assumption the response of the flow to the presence of mesoscale orography depends primarily on the maximum mountain height. However, when the topography is scaled to the resolution of NWP model, the total volume is conserved rather than the maximum height. The model orography is obtained from averaging of real orography over the area of grid-box and obviously the difference between model and real orography can be significant, especially in case of very high localised peaks that does not contribute much to averaging. Consequently, the volume of unresolved orography is not taken into account by dynamics of the model. Another argument was the observation that air in the deepest valleys

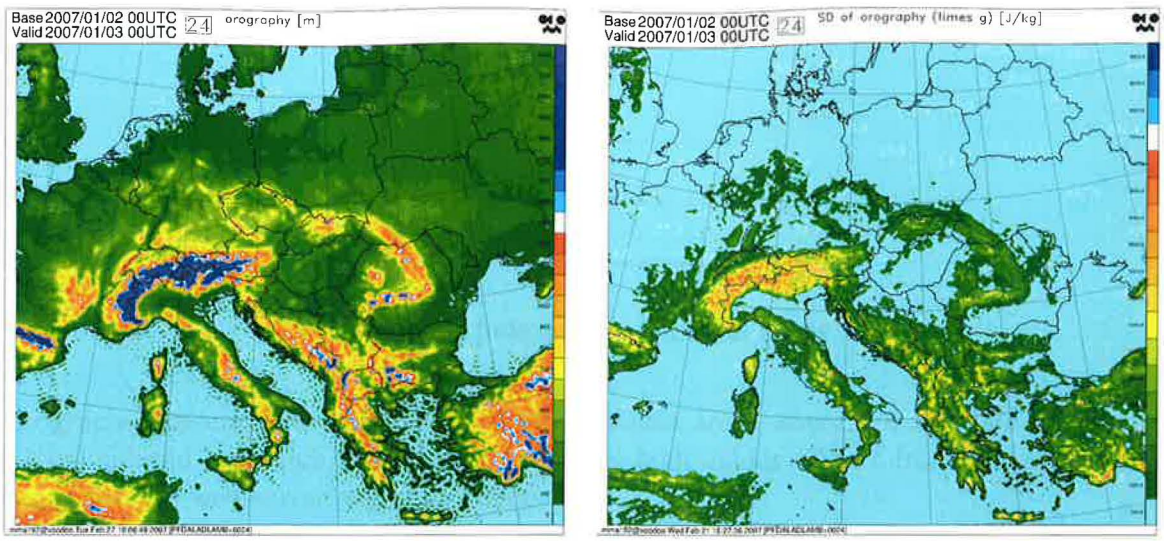

(a) (b)

Figure 2.2: (a) mean model orography height and (b) standard deviation of orography times g in ALADIN CHMI.

is often decoupled from the flow in higher altitudes, suggesting that the effective volume of the orography, as seen by large scale flow, should contain also the one of the valleys. This may explain why the early results with enhanced orography were so successful.

The envelope method of representation of sub-grid orography is based on artificial increase of the mean height of model orography adding an increment proportional to the standard deviation σ of the local subgrid scale orography

$$h_{env} = h_{mean} + \gamma \, . \, \sigma(h)$$

where γ is an empirical coefficient of order one ($\gamma = 1$ in the ALADIN/ARPEGE framework). In Fig. 2.2 the mean model orography of ALADIN CHMU together with standard deviation of subgrid orography is presented.

This very heuristic approach of representing a subgrid orography works surprisingly well providing the following useful benefits:

- additional volume effect of sub-grid scale orography giving better global wave patterns
- it simulates the upstream blocking of the flow impeding a mountain (non-local 3D effect which is hard to parametrise along the vertical and for which there is presently no other solution)
- stagnant valley air isolation and its additional contribution to the volume effect

Although the concept of envelope orography is very simple, it was quite successful and was implemented in many models during several years in the eighties. However, an envelope orography brings also some disadvantages. The problem of this method is an inexact description

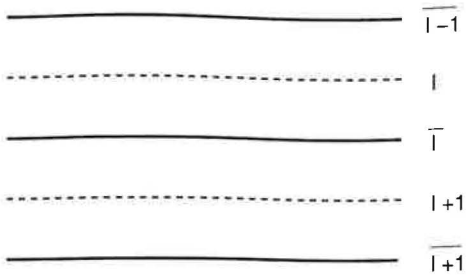

Figure 2.3: Indexation of vertical levels.

of orography especially at the borders of mountainous areas where the standard deviation of the local subgrid orography can acquire relatively high values. Apart from others, the most pronounced and well known negative effects are:

- overestimated precipitation rate at the windward sides of the mountains
- too strong Föhn effect
- some synoptic observation stations end up below the model's surface causing problem in data assimilation process

Additionally, the boost of more complex parametrisation schemes in the beginning of the nineties led to rapid fade out of this method in many NWP models including ALADIN, not to mention that its physical justification is more and more difficult. Unfortunately, the removal of envelope orography in ALADIN/ARPEGE can still not be considered as fully solved. A transition from envelope to mean orography results in not negligible reduction in forecast quality, especially for surface quantities. Therefore even today many ALADIN partner countries still use an envelope in their operational suite.

2.3 ALADIN/ARPEGE GWD parametrisation scheme

2.3.1 Model setup

In dynamical part of model the terrain-following hybrid vertical coordinate η is used. However, in the physical parametrisations the pressure coordinate is used instead. The main model variables (e.g. temperature, geopotential, wind components, moisture) are computed at *full levels* which are enumerated from the bottom to the top by $L..1$ representing the middle of model layer. The vertical fluxes (e.g. of heat, horizontal momentum) are computed at *half levels* which are indexed with a bar ranging from $\overline{L}$ to $\overline{0}$. As one would expect, they represent interfaces between two model layers.

2.3.2 Surface stress

The two main objectives of GWD parametrisation schemes are to evaluate the surface pressure drag and vertical distribution of the horizontal momentum flux induced by gravity waves. In this Section, we will deal with the former one. The surface drag in the ALADIN/ARPEGE framework is expressed following an early (and approximate) proposal of Boer et al. (1984), suggesting a formula

$$\tau_s = \rho_s \kappa N_s U_s h \tag{2.1}$$

with κ a non-dimensional tunning coefficient, surface wind U_s, Brunt-Väisäla frequency N_s, surface density ρ_s and the standard deviation of unresolved orography h. However, the linear theory of stationary waves in case of uniform flow over 2D bell-shaped mountain rather dictates h^2-dependency given by

$$\tau_{lin} = \rho K N U \mathcal{H}^2 / L \tag{2.2}$$

with K being equal to $\pi/4$ in this idealised case, $\mathcal{H}$ effective mountain height in z-coordinates ($\mathcal{H} = Rh$) and L characteristic horizontal dimension of the mountain. This expression is generally agreed to be valid for cases with no blocking effect when $F < F_c$ (see Sec. 2.3.8 for more details). For parameter regime with $F > F_c$ the wave-drag part may be computed identically assuming LM97 argumentation that separation surface between blocked flow part and wave-inducing is fully fluctuating or $\mathcal{H}^2$ may be replaced by T^2 in expression for τ_{lin}, where $T = \mathcal{H}F_c/F$ is wave-generating depth (WBCJ03). In ALADIN/ARPEGE scheme we admit that neither of the two extreme hypotheses (the flat or fully fluctuating wave-separation surface) is true choosing a "geometrical" intermediate for τ_{lin} replacing $\mathcal{H}^2$ by $\mathcal{H}T$ thus leading to the following expression for the wave-drag induced stress magnitude

$$\tau_w = \frac{F_c}{F}\tau_{lin} = \rho K N U \mathcal{H} T / L = \rho \frac{K F_c U R}{N L} N U h, \tag{2.3}$$

which is similar to our previous expression (2.1) with linear dependency upon obstacle height, but this time with

$$\kappa = \frac{K F_c U R}{N L} \tag{2.4}$$

becoming a physical constant since $NL/U = const.$

However, this type of justification cannot extend to the case $F < F_c$. There one must return to the linear results. In order to stay compatible with the previous version of the scheme and not to touch also anisotropy, deposition, resonance and trapping issues, this is done by replacing κ by $\kappa' = \kappa F/F_c$ in expression for τ_w to get the wave-induced stress equal to τ_{lin} (see (2.3)). Although it is not exact solution, it may be judged as fully consistent and well approximated giving relatively weaker values of drag in such situations.

2.3.3 Low level averaging

Both expressions (2.1) and (2.2) in the previous Section were derived assuming uniform flow and stability conditions. Thus we have to make a proper choice for surface quantities that

would be representative for mountain wave generation depth. However, we cannot use actual surface wind because of its imposed boundary condition (wind is always zero at the surface). Additionally, arbitrary choice of the lowest (or several) model layer(s) would introduce a substantial dependency on the resolution of vertical discretization. To overcome this problem, we compute *effective surface values* which are kind of average over a depth which depends on the sub-grid scale mountain height. This *effective obstacle height* (in pressure coordinates) can be expressed as

$$\mathcal{H}_p = \min\left\{p^{\overline{L}} - p^1,\ \max\left\{R\ \rho_s\ g\ h,\ p^{\overline{L}} - p^L\right\}\right\} \tag{2.5}$$

with R a tunable parameter ($R = 3$ in ALADIN). Thus the effective obstacle height is at least the pressure difference between the surface $\overline{L}$ and the lowest model level L and at most the highest model level 1. The effective surface wind and Brunt-Väisäla frequency are averaged over the height $\mathcal{H}_p$ giving

$$\mathbf{v}_s = \sum_{L}^{1} W^l \mathbf{v}^l \tag{2.6}$$

$$\mathcal{N}_s = \sum_{L}^{1} W^l \left(\frac{N^2}{\rho g}\right)^l \tag{2.7}$$

where $\mathcal{N}$ is normalized squared Brunt-Väisäla frequency (to preserve pressure-scale additivity of the potential temperature vertical increments) with the following weights

$$W^l = \max\left\{0,\ \frac{p^{l+1} - \max(p^l,\ p^{\overline{L}} - \mathcal{H}_p)}{\mathcal{H}_p}\right\}. \tag{2.8}$$

Hence, values from corresponding levels are accounted proportionally to the thickness of the layer (in pressure units). The upward summations in (2.7) are actually stooped as soon as $W^l = 0$. As the subgrid obstacle height may extend beyond several model levels, the wind an Brunt-Väisäla frequency are modified below $\mathcal{H}_p$ in order to avoid discontinuities, taking linear combination of their surface values $(u_s, v_s, \mathcal{N}_s)$ and their actual values $(u^l, v^l, \mathcal{N}^l)$ thus finally giving effective surface wind $\mathbf{v}_l$ and effective Brunt-Väisäla frequency $\mathcal{N}_l$

$$\mathbf{v}_l = \mathbf{v}_s\left(1 - \frac{p^{\overline{L}} - p^l}{\mathcal{H}_p}\right) + \mathbf{v}^l\ \frac{p^{\overline{L}} - p^l}{\mathcal{H}_p} \tag{2.9}$$

$$\mathcal{N}_l = \mathcal{N}_s\left(1 - \frac{p^{\overline{L}} - p^l}{\mathcal{H}_p}\right) + \mathcal{N}^l\ \frac{p^{\overline{L}} - p^l}{\mathcal{H}_p}. \tag{2.10}$$

2.3.4 Anisotropy

Additional complexity arise when one wants to take into consideration also directional effects due to anisotropy of the unresolved orography. The sub-grid scale obstacles in GWD

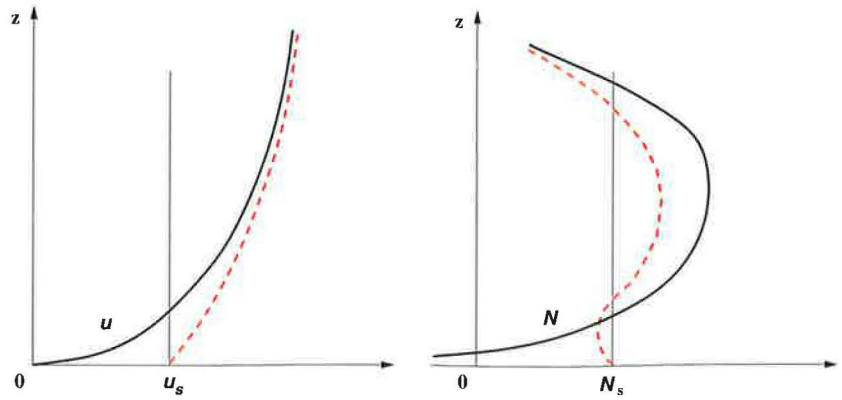

Figure 2.4: Profiles of (left) effective wind and (right) effective normalized squared Brunt-Väisäla frequency after surface value computation and linear recombination within effective obstacle height.

parametrisation are represented as elliptic shape mountains where anisotropy is determined by γ the ratio of eigenvalues of unresolved orography variance tensor. Here, unlike in isotropic case, the surface stress is generally no longer exactly opposite to the incident surface wind and can have generally a different direction. This is substantial difference from isotropic case where we implicitly assumed that surface stress is parallel with (but opposite to) the surface wind velocity. Most schemes incorporating anisotropy, including the one described here, are based on the theory of Phillips (1984) which allows us to write the surface stress in case of elliptic mountain as

$$\vec{\tau}_s = \sigma U[-(B\cos^2\psi + C\sin^2\psi)\vec{l} - (B-C)\sin\psi\cos\psi\vec{m}] \tag{2.11}$$

where ψ is angle between the surface wind vector and minor axis of the ellipse, U the real wind, $\vec{l}$ and $\vec{m}$ unit vectors respectively parallel and perpendicular to the wind, σ a constant and B and C functions of complete elliptic integrals of the first and second kind. Further, we introduce *fictive surface wind* which is defined as the wind that would correspond in the isotropic case to the above derived anisotropic surface stress and is expressed as

$$u_{fs} = Au_s + D(u_s\cos 2\psi + v_s\sin 2\psi) \tag{2.12}$$
$$v_{fs} = Av_s + D(u_s\sin 2\psi - v_s\cos 2\psi) \tag{2.13}$$

where A and D are defined as

$$A = \frac{2}{\pi}(B+C) \qquad \text{and} \qquad D = \frac{2}{\pi}(B-C)\,, \tag{2.14}$$

or alternatively using analytical fit to the elliptic integrals

$$A = \gamma^4 + \frac{1}{2\pi}[4(1-\gamma^2)(1+\alpha_1\gamma^2) - \gamma^2\ln(\gamma^2)(1+\alpha_2\gamma^2)] \tag{2.15}$$
$$D = \frac{1}{2\pi}[4(1-\gamma^2)(1+\delta_1\gamma^2) + 3\gamma^2\ln(\gamma^2)(1+\delta_2\gamma^2)] \tag{2.16}$$

with

$$\alpha_1 \simeq 1.44 \quad \alpha_2 \simeq 0.22 \quad \delta_1 \simeq 0.67 \quad \delta_2 \simeq 0.44 \, .$$

Finally, after all above computations, the Boer's formula for the surface stress becomes

$$\vec{\tau}_s = \kappa \rho_s N_s \vec{v}_{fs} h \, . \tag{2.17}$$

2.3.5 Upper level deposition

In the previous Section we have presented how a qualitative estimate of the vertical momentum flux due to gravity waves generated by the elliptic mountains is obtained. However, the amount of this flux is not constant throughout the whole atmosphere and can be significantly modified. In Chap. 1 we could see that gravity wave drag is directly related to the vertical divergence of the momentum flux, thus proper representation of the processes that lead to the changes of this flux with height is the essential part of the GWD parametrisation scheme.

Momentum flux for the wave of amplitude a and wavelength can be written as λ

$$\tau = -\rho N U \frac{a^2}{\lambda}. \tag{2.18}$$

In the absence of wave breaking (which is not necessarily true in a real atmosphere), one can impose a hypothetical constant value of τ in order to see how amplitude a has to change as a function of N, U, and ρ. We can see that there are essentially three processes that lead to the amplifying of a wave amplitude. The first one is so called "density effect" (ρ decreases with height) which leads mainly to the deposition of the waves in the stratosphere. The second process is related to the decrease of stability and will be discussed in more detail in the one of the next Sections. The last mechanism is embodied in the *Eliassen-Palm theorem*, which states that for a steady wave field in the absence of dissipation, the vertical flux of horizontal momentum is independent of height except at levels where the mean wind U is zero. However, the breaking does not only occur when the wind velocity vanishes, but also when the wind turns with height, i.e. when the higher level wind projected on the fictive wind goes to zero, with full extinction of the wave when

$$U = \frac{\vec{v}.\vec{v}_{fs}}{\|\vec{v}_{fs}\|} = 0. \tag{2.19}$$

In the atmosphere, all these processes can eventually lead to overturning of the waves and absorption by turbulence. Thus waves deposit their momentum flux at this *critical levels* generating mean flow deceleration.

Condition for wave breaking is embodied in the Lindzen's saturation theory (Lindzen, 1981) which states that wave breaking occurs when the amplitude of the wave equals its wavelength and resulting turbulent adjustment maintains the isentropes exactly vertical. Furthermore, he showed that under these constraints, the associated *saturated momentum flux* obeys the following proportionality rule

$$\tau_{sat} \sim \frac{\rho U^3}{N}. \tag{2.20}$$

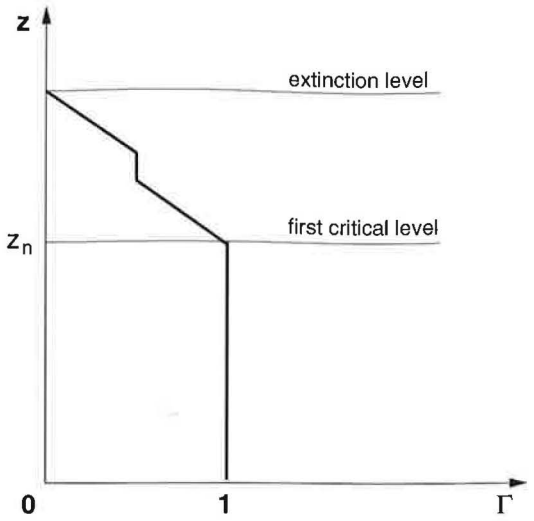

Figure 2.5: The vertical profile of function Γ in case of saturation.

However as one can note, we are missing absolute value of the above expression. Thus we make an assumption that the momentum flux at the surface is just saturated and can be expressed the same way using (2.20). Although this hypothesis is not fully correct, it provides acceptably approximate solution to this scaling problem.

The computation of the vertical variation of the momentum flux is done from the surface to the top of the atmosphere. For each level we compute the value of saturation flux which is compared to the value immediately below. If this flux exceeds the saturation one, the waves are assumed to break and the flux is adjusted to the saturation value, otherwise we keep the value unchanged. In our parametrisation, we define the ratio between the saturation flux at arbitrary level to the surface one

$$\gamma_l = \frac{\rho_l}{N_l}\frac{N_s}{\rho_s}\left(\frac{U_l}{U_s}\right)^3 \tag{2.21}$$

then we get for the flux at half level l

$$\vec{\tau}_l = \Gamma_l \, \vec{\tau}_s \tag{2.22}$$

where

$$\Gamma_l = \max(0,\ \min(\gamma_l, \Gamma_{l+1})) \tag{2.23}$$

is surface flux proportionality factor. If Γ_l gets null or negative, we reset it to zero for all levels above, as the waves have been totally absorbed and flux disappeared.

2.3.6 Resonance

In the previous Section we have described deposition of the gravity wave induced momentum flux at the critical levels, however we did not consider possible reflection of the waves and

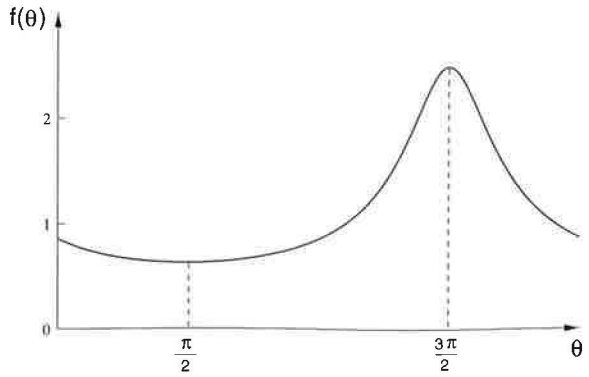

Figure 2.6: The resonance function $f(\theta)$.

their consequent interference with the incident waves. Based on the work of Peltier and Clark (1984), the resonant amplification can occur when the reflected wave is in phase with the incident one. They showed that constructive interference occurs when the critical (reflection) level is situated at height

$$z_c = \left(\frac{3}{4} + k\right)\lambda \tag{2.24}$$

where k is an integer. For vertically propagating waves with large horizontal wavelength, assuming U and N constant, we can write $\lambda = 2\pi\frac{U}{N}$ (see Chapter 1). The above resonance condition then becomes

$$\frac{U}{N}z_c = \frac{3}{2}\pi + 2k\pi \tag{2.25}$$

which in this form expresses the phase shift for the case of constant vertical profiles of wind and stability. For the continuously stratified flow the corresponding phase shift can be expressed as

$$\theta = \int_0^{z_c} \frac{U}{N} dz. \tag{2.26}$$

or equivalently in discrete form (which is used in ALADIN/ARPEGE)

$$\theta = \sum \frac{U}{N}\frac{\Delta p}{\rho g}. \tag{2.27}$$

In the next, we define a periodic resonance function $f(\theta)$ with average value 1 and which acquires a maximum value at $\theta = 3\pi/2$ (amplification) and minimum at $\theta = \pi/2$ (destruction). The expression for resonance function is determined under the consideration that reflected wave will undergo several reflections between ground and critical level which allows us to write it as

$$\begin{aligned} f(\theta) &= |1 + K_a e^{i(\theta-\theta_0)} + K_a^2 e^{2i(\theta-\theta_0)} + \cdots| \\ &= \left|\frac{1}{1 - K_a e^{i(\theta-\theta_0)}}\right| \end{aligned} \tag{2.28}$$

where K_a is an empirical parameter associated to a damping of the reflected waves ($K_a = 0.6$ in ALADIN/ARPEGE). Since $f(\theta)$ has maximum at $\theta = \frac{3\pi}{2}$, one finds that $\theta_0 = \frac{3\pi}{2}$. The

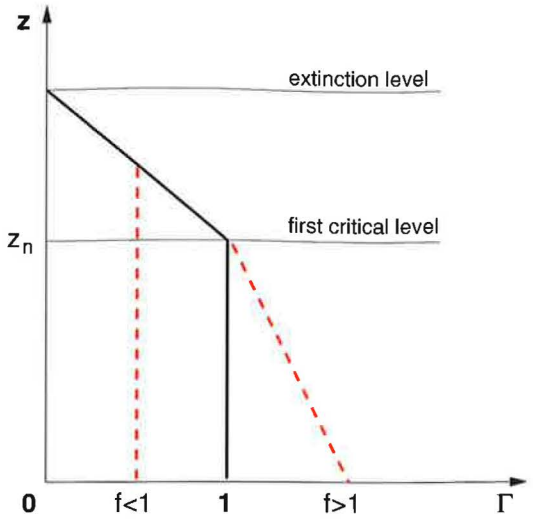

Figure 2.7: Correction of proportionality factor Γ (red dashed line) in case of resonance for both amplification ($f > 1$) and destruction ($f < 1$) of the waves.

resonance function can be finally rewritten as

$$f(\theta) = [1 - K_a^2 + 2K_a \sin(\theta]^{-\frac{1}{2}} \, . \tag{2.29}$$

For simplicity, we take into account only the resonance under the first critical level neglecting possible interferences between the remaining existing reflection levels. At first the corresponding phase shift θ and resonance function $f(\theta)$ are calculated. When $f(\theta) < 1$ we apply the same reduction factor $\Gamma_l = f(\theta)$ for all levels below the critical one (since drag cannot increase with height) to simulate reduction of the drag due to wave destruction. On the contrary, when $f(\theta) > 1$ the waves are amplified which enhances the drag below the critical level, so at the surface we set $\Gamma_L = f(\theta)$. However, not much is known about the exact profile of the drag between the surface and the critical level so we heuristically use a linear interpolation

$$\Gamma = \Gamma_L \frac{p^{\bar{l}} - p^{crit}}{p^{\bar{L}} - p^{crit}}. \tag{2.30}$$

The resulting profile of proportionality factor Γ for both cases is shown in Fig. 2.7.

2.3.7 Wave trapping

If the stratification of the atmosphere becomes unstable at higher levels, the waves are prevented from passing through (as they cannot be sustained in conditions with negative value of N) and are reflected back undergoing several reflections between the ground and instable layer. These "trapped" waves can travel long distances downstream where they eventually deposit their momentum thus exerting a drag at large distances which would in fact require a three-dimensional parametrisation scheme to account for this effect. However, this would bring a great complexity in conjunction with the impact in the host model. Nevertheless, in

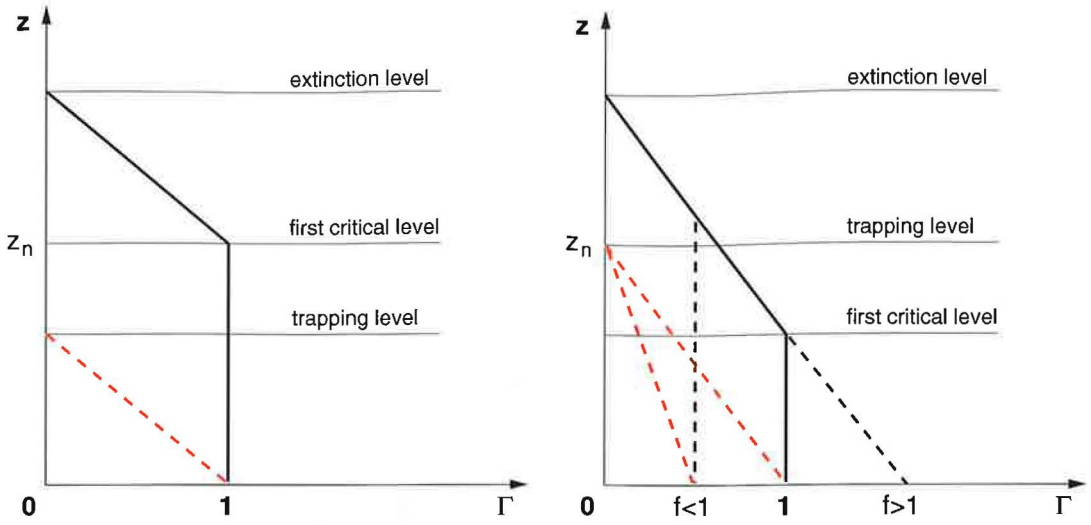

Figure 2.8: Correction of proportionality factor Γ (red dashed line) in case of wave trapping.

order just to not neglect the trapping effect, the associated drag will be also parametrised along the single vertical column.

Similar to the case of resonance, we consider only the lowest trapping level. However, here the assumption is more accurate as the waves cannot be sustained when $N < 0$ and are completely decayed which is not the case of saturation at critical levels. Depending on the configuration of the trapping and critical level, we distinguish two cases. When trapping level is below the first critical level, no resonance can occur and $f(\theta)$ is set to 1. Otherwise, when the trapping level is above the critical one, the resonance function $f(\theta)$ is restricted to not exceed the value 1. Then, in the similar spirit to the case of resonance we heuristically make a linear interpolation between the surface and trapping level

$$\Gamma_l = \Gamma_L \frac{p^l - p^{trap}}{p^L - p^{trap}}. \tag{2.31}$$

The schematic picture of the method is showed in Fig. 2.8.

2.3.8 Blocked flow

Up to now, we have been concerned only with a gravity wave drag part of the parametrisation. However, most of the present schemes try to represent also the drag exerted by the unresolved orography on the low-level mean flow.

In conditions of strong stratification and relatively weaker wind velocities, the kinetic energy of the low level flow does not have to be sufficiently large to overcome the potential barrier induced by the stable stratification and part of the flow has to separate and go around the obstacle. The characteristic of the flow regime over the obstacle in the presence of stratification is usually measured in terms of *Froude number*

$$Fr = \frac{U}{NH} \tag{2.32}$$

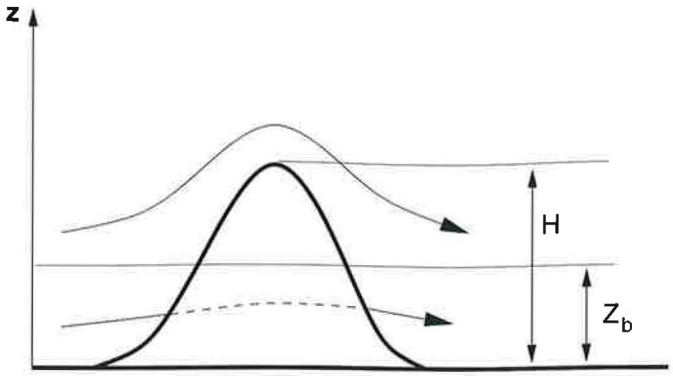

Figure 2.9: Schematic description of the flow separation. The air below Z_b has to contour the obstacle. See the text for more explanation.

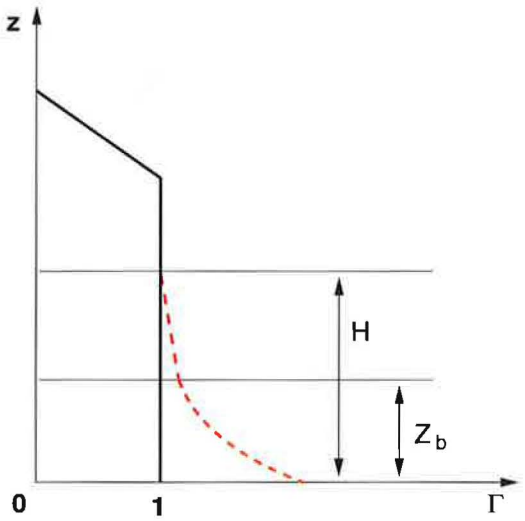

Figure 2.10: The correction of momentum flux (red dashed line) within sub-grid scale mountain height H accounting for the form drag.

which is basically the ratio of kinetic energy of the incident flow and potential energy of the air parcel when it gets over the top of the mountain. However, this result is only approximate because it does not take full account of the dynamics, but it is a good guide. In the framework of ALADIN/ARPEGE GWD parametrisation scheme, the *inverse Froude number* $F = NH/U$ is used rather than the "classical formulation" and can be also understood as non-dimensional (or normalised) mountain height. The flow is assumed to be blocked when F exceeds a critical threshold value $F_c = 0.5$. In order to take into consideration the ellipticity of the mountain, the inverse Froude number is actually computed in yet another way, being compatible with the results of Sect. 2.3.4, as

$$F = \frac{N\mathcal{H}U_{fs}}{U_s^2} \tag{2.33}$$

Let's consider a sub-grid mountain with height $\mathcal{H}$ and we further assume flat separation surface between the blocked part of the flow and the wave-inducing one. If the condition for blocking is fulfilled, the height of the blocked flow can be expressed, after some straight

forward computations, as

$$Z_b = \mathcal{H} \max\left(0,\ 1 - \frac{F_c}{F}\right). \tag{2.34}$$

Below Z_b the flow will be forced to go around the mountain and will "feel" additional surface type drag exerted by the mountain. This *form drag* can be written as

$$\vec{D}_b(z) = -\rho C_d l(z) \frac{\vec{v}\|\vec{v}\|}{2} \tag{2.35}$$

with C_d an adimensional aerodynamic drag coefficient of dimension one and where $l(z)$ represents the horizontal width of the obstacle as seen by the flow at a height z. For an elliptical mountain, this width can be expressed (according to LM97) as

$$l(z) = X\sqrt{\frac{Z_b - z}{\mu + z}} \tag{2.36}$$

where X is the horizontal length scale of the grid point region and μ is a slope parameter. However, as ALADIN/ARPEGE doesn't use slope, it has to be replaced by some rough evaluation. The total drag on the mountain is then given by the integration of (2.35) between 0 and Z_b where integral of $l(z)$ can be approximated by the expression

$$\sqrt{\frac{\left(1 - \frac{z}{Z_b}\right)^3}{1 + \frac{\alpha z}{\mathcal{H}}}}. \tag{2.37}$$

The additional form drag is then represented introducing adaptation of multiplying coefficient Γ_l by a factor linked to this effect

$$\Gamma_l = \Gamma_l \left(1 + a_d \sqrt{\frac{\left(1 - \frac{z}{Z_b}\right)^3}{1 + \frac{\alpha z}{\mathcal{H}}}}\right) \tag{2.38}$$

where

$$a_d = C_d \frac{\|\vec{v}_{fs}\|}{\mathcal{H} N_s} b_d \qquad \text{and} \qquad b_d = \max\left(0,\ 1 - \frac{F_c}{F}\right).$$

2.3.9 Lift force

The purpose of this Section is to introduce a parametrisation of sub-grid mountain volume effect due to terrestrial rotation which modifies the vorticity in the process of vortex compression to keep the potential vorticity unchanged, resulting in the deviation of the flow in the vicinity of the obstacle. Associated circulation over the obstacle is driven by the force which is proportional to the mountain volume and whose horizontal component is perpendicular to

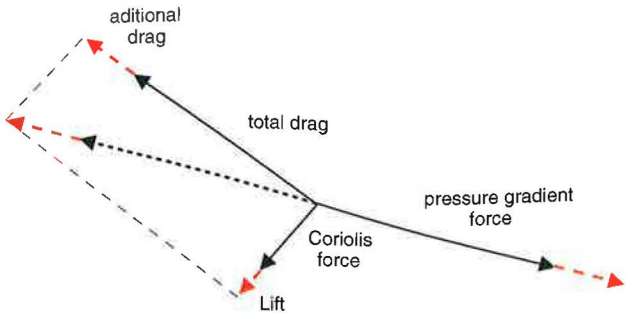

Figure 2.11: Graphical description about how the lift effect amounts to increase the total drag (form-drag plus wave-drag in our idealised case) by the same proportion as the basic lift effect adds to the Coriolis force in the case of geostrophically balanced flow. The sizes of the arrows are completely arbitrary.

the incident flow. This effect was previously included in the concept of envelope orography (as the volume of the orography was artificially increased) and was thus explicitly resolved by dynamical part of the model. However, if one wants to represent this effect in non-envelope case, it has to be parametrised introducing a *lift force* [1] as a new substitute for the missing volume effect of the unresolved orography.

Lott (1999) proposed the lift parametrisation as a doubling of Coriolis effect in proportion to the volume of sub-grid scale mountain. The lift force is applied on a volume of the air between the ground and $\mathcal{H}$ and varies according to $(1-z/\mathcal{H})/(1+\alpha z/\mathcal{H})$ which is the assumed shape of the sub-grid mountain with α the mountain shape parameter. Then, the additional Coriolis-complementing lift force contribution can be expressed by defining an equivalent to the Coriolis parameter f as

$$f' = L_t f \frac{\alpha^2 \frac{1-z/\mathcal{H}}{1+\alpha z/\mathcal{H}}}{R((1+\alpha)ln(1+\alpha)/\alpha)} \quad \text{for} \quad z < \mathcal{H} \tag{2.39}$$

with R defined as previously $\mathcal{H}/h$ and L_t a tunning coefficient for which Lott gives a theoretical value one. The normalization factor $\alpha^2/((1+\alpha)\ln(1+\alpha)/\alpha)$ insures that $f'(z)$ averaged over a depth $\mathcal{H}$ is equal to the basic Coriolis effect (assuming $L_t = 1$). Practically, the lift force has the same effect, as if the Coriolis factor was artificially increasing to $f + f'$. The resulting wind tendencies are given by

$$\frac{\partial u}{\partial t} = +f' \frac{v - u\Delta t f'/2}{1+(\Delta t f'/2)^2} \tag{2.40}$$

$$\frac{\partial v}{\partial t} = -f' \frac{u + v\Delta t f'/2}{1+(\Delta t f'/2)^2}. \tag{2.41}$$

The above obtained solution is meant to physically represent a purely Coriolis-like effect and is thus parametrised orthogonally to the wind vector. However, it always created problems to introduce the lift at higher horizontal resolutions (especially in LAM ALADIN) i.e. where distinction between actual and geostrophic wind becomes more important. According to Geleyn et al. (2006), the above mentioned strange behaviour was attributed to the fact that only

[1] This term was adopted from the aerodynamic lift force associated to the flow over a wing profile, however, this term is partially misleading as the forcing principle is obviously different.

the non-working part of the lift effect was previously used, while the basis of the theory, on which Lott relies, assumes geostrophically balanced flow. Hence, if one assumes that turbulent and convective drag terms are negligible compared to the mountain drag ones, the lift effect should amount to increase the pressure drag force (form and wave drag) by additional f'/f-proportional contribution (see Fig. 2.11) within the depth $\mathcal{H}$ above the ground, which is in accordance with work of Ólafsson and Bougeault (1997) who found that taking rotation into account leads to increase of drag. Then, one can write

$$\tau = \tau_w + \left(1 + \frac{f'}{f}\right)\tau_f \tag{2.42}$$

Nevertheless, to introduce lift force at the model levels below the subgrid mountain height $\mathcal{H}$ is in many aspects different from what actually happens in the process of vortex compression. In reality, each isentrope passing over the obstacle is displaced by the amount proportional to the mean mountain height and thus lift force is also transmitted vertically. From this point of view the lift parametrisation discussed here is quite "crude". However, the vertical repartition of the lift effect is too complex to be implemented in a hydrostatic model, except by changing the lower boundary height (as is done in envelope orography concept).

2.3.10 Isolation of some part of the flow

The envelope effect (to be substituted by the lift part of the scheme) posses with one additional aspect that is not embodied in our parametrisation, and that is the one concerning the sub-grid valley air isolation (in nature the volume unseen by the large scale flow is rather that of the valleys). Indeed, the air in the valleys neither fully influences the flow characteristics nor feels the drag effects.

One therefore elects geometrical representation of the "unseen flow" by introducing a vertical profile βS (with S assumed shape of sub-grid mountain and $\beta = 0.5$ in ALADIN/ARPEGE) that is eliminated from low-level averaging process that leads to evaluation of the surface values of wind and Brunt-Väisäla frequency (see Geleyn et al., 2005). Hence, we have reduced the influence of diurnal cycle. The same β-portion is also filtered out from the impact of drag in lower layers as the drag does not act on the air that does not contribute to it. As the influence of the lower layers is reduced, the resulting estimate of surface wind tends to increase which in turn amplifies the linear part of the surface drag.

2.3.11 Numerical aspects

Apart from the non-working lift force, which needs no stability considerations, an implicit treatment of the horizontal momentum equation due to orographic drag is advisable to obtain a robust scheme independent on the length of time and space discretization steps. However, as the routine described here returns fluxes and the resulting tendencies are computed in a different subroutine where one formally uses explicit discretization of the tendency equation

$$\frac{\partial U}{\partial t} = -g\frac{\partial \tau}{\partial p}, \tag{2.43}$$

some adaptations have to be done so that final recomputations are equivalent to an implicit formulation.

The computation of effective surface wind from lower levels velocities and the surface characteristics could hide an implicit evolution equation, which, if not handled cautiously, could become unstable. All momentum fluxes are proportional to $U_s = \frac{\vec{v}_s.\vec{v}_{fs}}{\|\vec{v}_{fs}\|}$ the projection of the surface wind on the fictive wind. One may find

$$\frac{\partial U_s}{\partial t} \sim \frac{\partial}{\partial p} \int_0^{\mathcal{H}} U_s du \tag{2.44}$$

or alternatively with proportionality factor

$$\frac{\partial U_s}{\partial t} = -\mathcal{K} U_s. \tag{2.45}$$

For large time steps, in presence of altitude gradients possibly higher than those at lowest level, this system could become unstable, hence an implicit formulation is needed

$$\frac{U_s^+ - U_s}{\Delta t} = -\mathcal{K} U_s^+. \tag{2.46}$$

Reordering the above equation, we get

$$U_s^+(1 + \mathcal{K}\Delta t) = U_s \tag{2.47}$$

giving

$$\frac{U_s^+ - U_s}{\Delta t} = -\frac{\mathcal{K}}{1 + \mathcal{K}\Delta t} U_s. \tag{2.48}$$

To get this split implicit formulation, we have to multiply all proportionality relations between τ_l and U_s by $\frac{1}{1+\mathcal{K}\Delta t}$.

In the following we will be concerned by discretization of the evolution equation (2.43) where $U = \frac{\vec{v}.\vec{v}_{fs}}{\|\vec{v}_{fs}\|}$. One should note that dependency on U is not linear because $\tau_l = \Gamma_l(U)\tau_s(U_s)$. To overcome this complexity, we consider the problem only as a vertical transport of horizontal momentum

$$\tau_l = \frac{1}{g} U_l \mathcal{M}_l \tag{2.49}$$

where $\mathcal{M}$ plays a role of a mass flux. Then discretization of equation (2.43) gives

$$\frac{U_l^+ - U_l}{\Delta t} = -\frac{U_l \mathcal{M}_l - U_{l-1}\mathcal{M}_{l-1}}{\delta p_l} \tag{2.50}$$

or

$$U_l^+ - U_l = -A_l U_l + A_{l-1} U_{l-1}, \tag{2.51}$$

defining $A_l = \frac{\mathcal{M}_\uparrow \Delta t}{\delta p_l}$ as the equivalent of a vertical Courant number. Discretising implicitly downwards

$$\begin{aligned} U_l^+ - U_l &= -\left(A_l U_l^+ - A_{l-1} U_{l-1}^+\right) \\ (1 + A_l)(U_l^+ - U_l) &= -A_l U_l + A_{l-1} U_{l-1} \\ &\quad + A_{l-1}(U_{l-1}^+ - U_{l-1}) \end{aligned} \tag{2.52}$$

leads to replace the flux τ by τ' according to

$$\tau'_0 = 0 \qquad \text{and} \qquad \tau'_l = \tau'_{l-1} - \frac{1}{1 + A_l}(\tau'_{l-1} - \tau_l). \tag{2.53}$$

Chapter 3

Experimental part

3.1 Downslope windstorm in the Tatras on 19/11/2004

3.1.1 Introduction

Cases, such as the one of downslope windstorm in the Tatras on 19/11/2004, offer an ideal opportunity to test capability and precision of numerical models to forecast such extreme events and at the same time, they often provide specific conditions that are appropriate for testing and tuning of miscellaneous model elements including physical parametrisations. Thus the situation in the Tatras was chosen as a primary case for studying unresolved orography effects and their parametrisation.

3.1.2 Synoptic situation and mesoscale conditions

On 19 November 00 UTC a positive upper air potential vorticity anomaly approached a strong surface baroclinic zone extended over northern Europe creating ideal conditions for generation of baroclinic instability. Shallow cyclone over central part of Germany underwent rapid development and propagated further westward approaching the borders of Czech Republic at 06 UTC. This rapid cyclogenesis was predicted many numerical models well before. At 12 UTC the cyclone moved over the southeastern part of Poland and at 18 UTC it was already situated over Ukraine. The associated cold front reached the northwestern borders of Slovakia at 11 UTC and at 13 UTC the line of the front crossed the region of High Tatras. Wind gusts in the High Tatras during the most intense phase of the windstorm activity were exceeding 40 m/s.

Stratification and wind profile are the most important elements in formation of favourable conditions for extreme mesoscale events such as downslope windstorms. However, there is no available aerological observation representative for the conditions on the windward side of the Hight Tatras at the time of windstorm activity. Hence, the properties of the flow had to be estimated from the ALADIN analysis. High wind shear and low stability at the lowest 800 m

above the ground created favourable conditions for generation of turbulence. This area was capped by inversion with significant increase of Brunt-Väisäla frequency in between 1500 and 2400 meters above sea level, just below the tops of the mountains. Although the corresponding Froude number was decreasing with height, it was still sufficiently large to support supercritical flow thus enabling the rising air parcels to accelerate along the slopes on the windward side of the mountains and generating a large amplitude lee waves. Such conditions are favourable for the onset of downslope windstorms.

Extensive case study of this severe event can be found in the work of SHV04, where high 2.5 km resolution tests are introduced comparing performance and quality of the forecast for hydrostatic and nonhydrostatic modes of ALADIN as well as dynamical adaptation. However, we are primarily concerned here by the quality of the operational forecast. The reference ALADIN SHMU operational run was (according to SHV04) using envelope orography with 9 km resolution. Synoptic scale features, such as rapid cyclogenesis, were well predicted and maximal wind gusts of 40 m/s were forecasted at the region of the High Tatras however, the horizontal distribution of the wind field was less precise and it was not possible to sufficiently localise the position of the event. The more interesting results were obtained for the runs without envelope orography that considerably underestimated the strength of wind gusts reaching peak values of only 20 m/s. Based on these results, one can conclude that at 9 km resolution with no envelope the model failed in forecasting of this extreme event. This was one of the challenging factors for further research in this case. However, after many tests of different settings using non-envelope orography, we were not able to "reproduce" this fail run. This can be the consequence of different physical parametrisation setup, not to mention that this specific case can be strongly sensitive on physical parametrisations, especially horizontal diffusion schemes, turbulence and subgrid scale orography schemes, and can eventually compensate each other. Hence, influence of parametrisations on the final forecast is probably very complex. Comparison of both, envelope and non-envelope tests with ALADIN CHMU can be found in Fig. 3.1. One can see some minor differences in maximal intensity of the wind gusts, but horizontal distribution remains roughly the same for both cases. Nevertheless, we soon realised that using the wind gusts as primary diagnosing variable is probably not the best choice because of its pseudo-random character.

3.1.3 Critical Froude number

Based on some earlier results of J. Vivoda (personal communication), there were some indications of relative improvement in magnitude and distribution of the wind field for the tests with increased critical Froude number Fr_c in comparison with the reference value of $Fr_c = 2$. This relatively surprising result became a direction indicator for our further research despite the fact, that this tuning constant was generally considered to be a well validated one. In our scheme, the form-drag is activated wherever the inverse Froude number F exceeds a threshold value $F_c = 0.5$ (or alternatively, when Froude number Fr is lower than a threshold $Fr_c = 2$). Hence increase of critical Froude number should obviously results in enlarging of the horizontal areas where the form-drag is applied which should consequently lead to decrease of surface wind. However, this is in contradiction with the above findings of J. Vivoda. Thus several tests have been performed in order to reveal the sensitivity of our scheme to this tuning constant and to confirm or disprove previously mentioned unexpected behaviour. For this purpose, we have

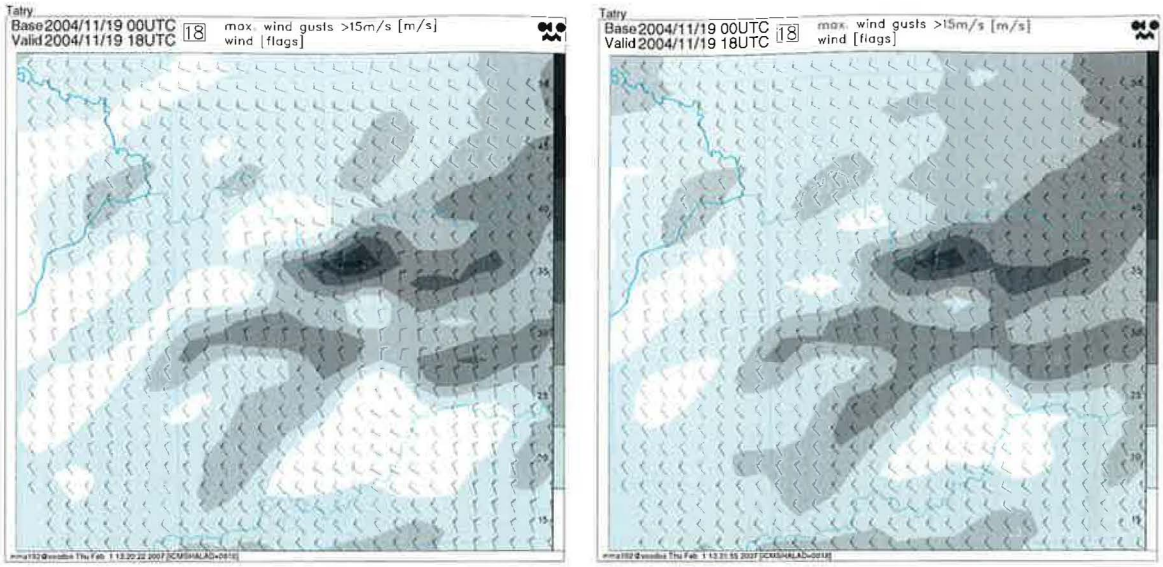

(a) (b)

Figure 3.1: Tatra case forecast with operational setting of ALADIN CHMI for (a) version with envelope and (b) without envelope orography.

decided to diagnose non-dimensional field of ratio F_c/F together with wind field at 500 m above the ground level (AGL) for both cases with and without envelope orography. The results can be found in Fig. 3.2 for three different settings of critical Froude number 1, 2, and 4 (or equivalently critical inverse Froude number 1, 0.5 and 0.25).

The field of F_c/F is intentionally truncated to maximal value of 2.5 because of extremely wide range of values that can be obtained. Especially at areas with very low unresolved orography height $\mathcal{H}$ and high wind speeds, the ratio F_c/F can acquire considerably high values that are not relevant for our study, as we are primarily interested in the effect of form-drag which is activated when the condition $F_c/F < 1$ is satisfied. We can see that there are no major differences between envelope and non-envelope case, though envelope case possesses slightly larger areas of blocking. Furthermore, after a closer look at the wind field one can note that enlarging the areas with form drag leads to a relative decrease in wind speed, which is in accord with our expectations. As we do not know a priori the exact amount of necessary blocking (through the form-drag) we can roughly estimate the reasonable amount of it taking into account the properties of the flow during the investigated event. Accounting the situation with low stability at lower layers, the setting with critical Froude number equal to 2 seems to be reasonable as the blocking effect will not be strong at this conditions. Hence, we are left with the previous well validated tuning of Fr_c.

3.1.4 Conclusions for the Tatra case experiment

In our experiments, the run with a new parametrisation could successfully forecast this severe event with no remarkable differences with respect to the one using envelope orography. Further, the above results also proved a physically consistent response of the scheme to the change of critical Froude number. As mentioned earlier, apart from GWD parametrisation, this case

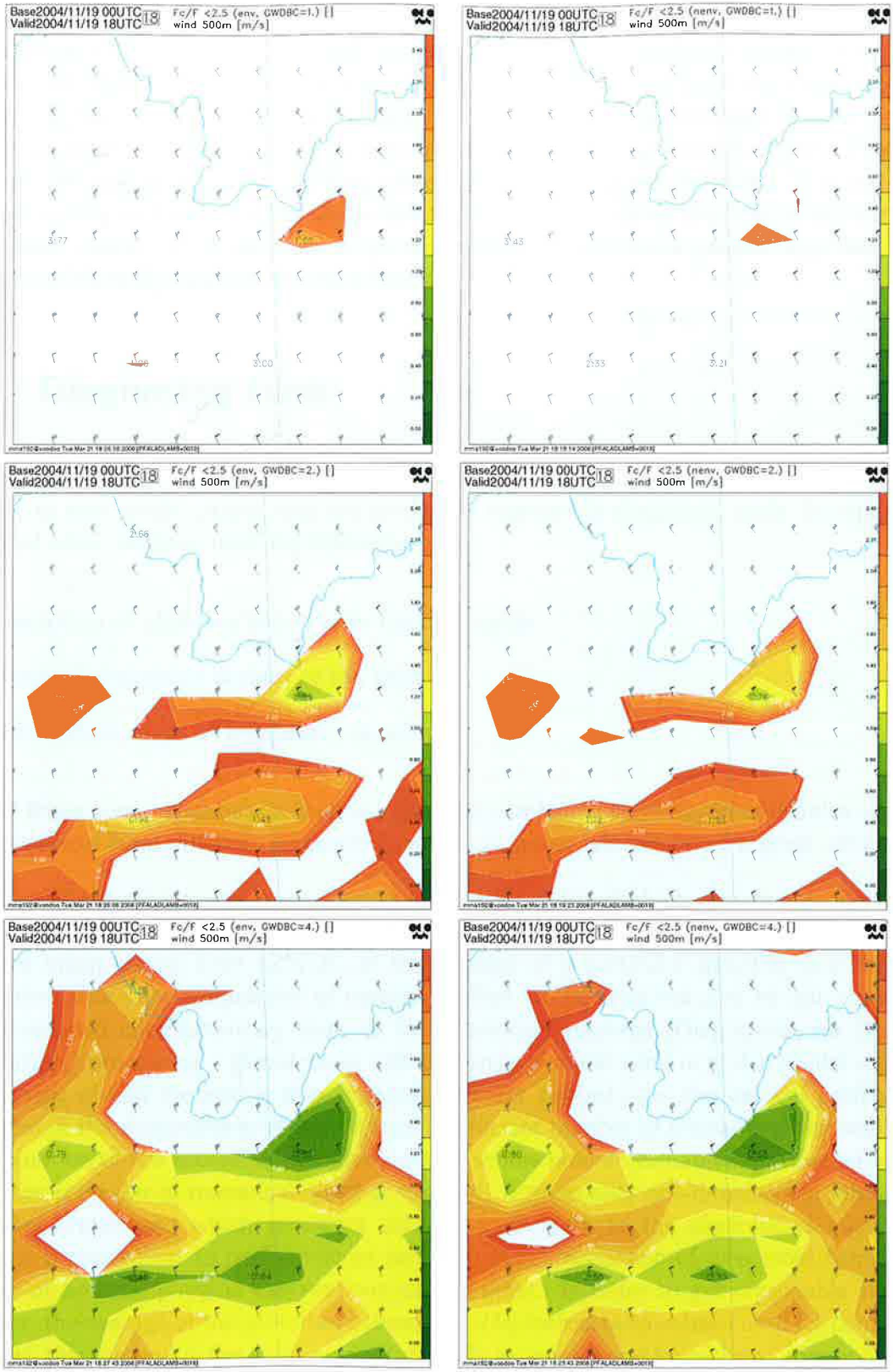

Figure 3.2: Non-dimensional parameter F_c/F and wind at 500 m AGL for several values of critical Froude numbers 1, 2 and 4 (top, middle and bottom panel respectively) and for both envelope (left panel) and non-envelope (right panel) case. Green contours indicate areas with form-drag acting.

can be very sensitive to different model setups (e.g. diffusion and turbulent schemes) and the resulting influence on the forecast can be therefore very complex. Despite many efforts, we were not able to reproduce the fail run of the Tatra case without envelope orography. Besides, we have soon realised that testing the GWD scheme on one specific case does not have to necessarily lead to overall improvement of the operational forecast quality. Even if one can tune the parametrisation obtaining perfect results for a particular event, it is not certain that this tuning will work for the whole spectrum of possible cases that can occur during the operational course. Thus we have to choose a different and more general approach to this problem which is discussed in the next Section.

3.2 Diagnosing tools

In order to better understand a behavior of GWD parametrisation scheme and the response of the flow to new modifications, one has to choose appropriate diagnostic tools. In experiments presented here, we have used the following ones:

- evolution of objective scores with forecast range
- vertical deposition profiles of the drag
- differential maps of prognostic variables

Each of these approaches has its pros and cons but combining them together enables us to look at the problem from different perspectives which is, as we will see later, a great advantage.

Evolution of objective scores is a statistical verification method which compares model forecast to the surface observations (SYNOP) and vertical soundings (TEMP) in the means of the bias and root mean square error (RMSE) of the average of a particular quantity over the whole integration area. For diagnostics of vertical profiles of the drag induced by our scheme, we have developed complementary tools to DDH software package (Diagnostics sur Domaines Horizontaux) processing a global mean 24h-tendency of zonal wind in global model ARPEGE. The benefit of this method is that it provides direct control over the vertical profile of the drag even in the stratosphere where we have insufficient number of measurements available for the evaluation of the scores. Although evolution scores provide valuable objective information about the precision of numerical weather forecast, it gives only one-dimensional information. To better understand which processes actually participate to the observed changes in the scores, it is convenient to perform some sort of spatial comparison of forecasted fields, as the number of possible physical explanations can be great. In order to get reasonable statistical estimate, the average of the set of ten subsequent 24h-forecasts have been used for comparison. However, this method is the most computationally expensive one from the all mentioned here.

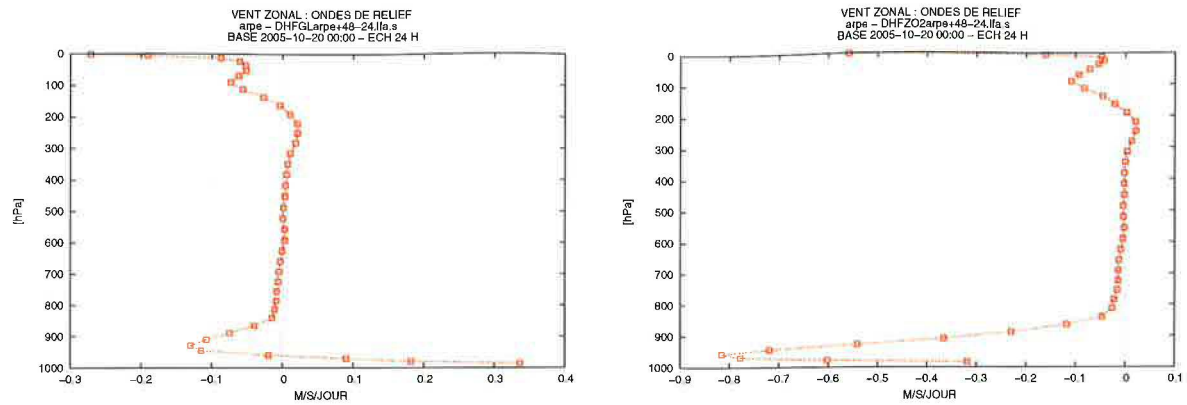

(a) (b)

Figure 3.3: Vertical profile of the drag induced by GWD parametrisation for (a) global average and (b) when taking into account only the average over the Norther hemisphere average.

3.3 Initial complications

To be assured that new complementary tools work properly and give the results that are in accord with the previous studies, the very experimental process has to be preceded by the phase of their testing. However, when diagnosing the vertical profile of the global averaged drag exerted by our parametrization on the zonal flow, we have encountered an unexpected result that the scheme is actually extensively accelerating the flow at lower levels (see Fig. 3.3a) which was a big surprise. This was firstly attributed to the existence of some bug in the current code. Surely, one could complain that a bug with such a large impact on the wind tendency should negatively influence the operational forecast to such an extend that it would be discover much earlier, but this does not have to be necessarily true because of the presence of various feedbacks that can lead to a compensation effects. For instance, if the mountain drag is reduced for some reason, the resulting increase of wind speed can be damped (to the certain extend) by additionally enhanced turbulence thus preventing the wind velocity from getting to a too high unrealistic values even with the incorrect internal representation of particular physical effects. This can make debugging a real nightmare. However, after a more detailed analysis of the problem, the explanation of the above mentioned inconsistency showed to be relatively simple. It resulted from the fact that in global averaging, drag exerted on the westerly flow correspond to deceleration and drag exerted on the easterly wind actually correspond to acceleration of the flow (depending on the definition of the zonal wind). Although the contribution of the former is usually dominating in the atmosphere, when averaged globally, surprisingly there might exist also opposite situations, which was exactly our case. Indeed, when we inspected the latitude-vertical cross section of the GWD scheme-induced drag, we found a localised area with extremely strong easterly wind over the Antarctic which might be a result of vortex-splitting (but this was not further verified). The above explanation was eventually confirmed when we plotted the drag profile averaged over the Northern hemisphere finally obtaining a correct result (see Fig. 3.3b). Thus solving this curious complication enabled us to proceed to the experimental part of the work.

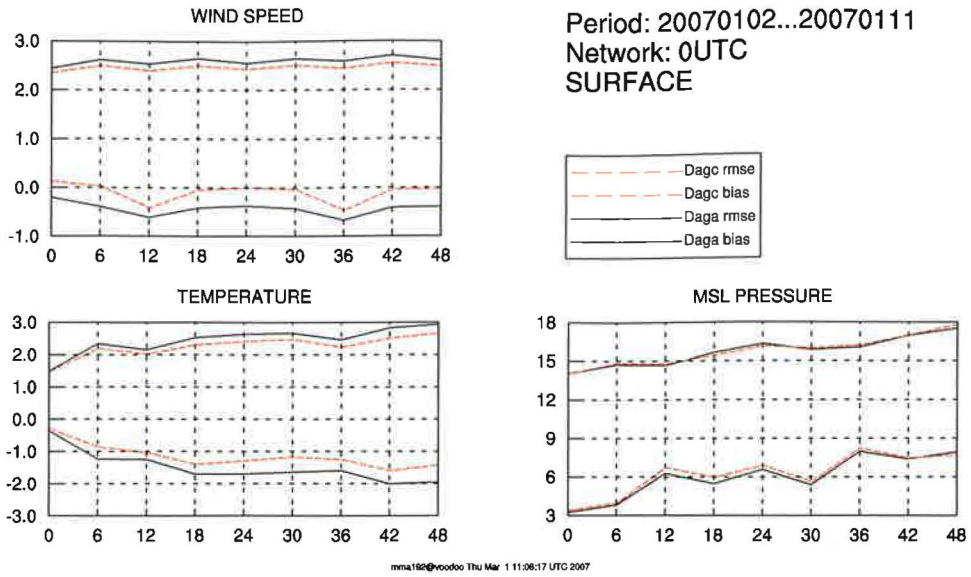

Figure 3.4: Comparison of evolution of scores for surface quantities between envelope (red dashed line) and non-envelope operational version of ALADIN (black solid line) computed for a ten day forecast period.

3.4 Analysis of envelope removal impacts

3.4.1 Objective scores

Before any changes to the current GWD parametrisation scheme are done, one has to take a closer insight to the effects of envelope orography to better understand all consequences of its suppression and to be able to propose appropriate modifications that would lead to physically consistent solutions. For this purpose, we can use an evolution of objective scores as the first analysing tool. In the following, we will be primarily concerned with comparing differences between the operational version of model ALADIN with the latest GWD scheme and parallel suite containing envelope orography with former GWD scheme setting. In Fig. 3.4 one can see that present drag parametrisation does not sufficiently substitute the effects of envelope. This problem is mostly evident for the surface quantities . We can see that current operational version has more negative bias and higher root mean square error (RMSE) in the surface wind as well as temperature. This behavior is not just coincidence. Lower temperature at the surface can be a direct consequence of reduction of turbulent mixing in lower layers due to decrease in wind speed. On the other hand, lower temperature at the surface increases stability that leads to higher form-drag within subgrid mountain height levels which further decelerates the flow. Thus temperature and wind are bound through the turbulence and stratification feedbacks. It is generally observed that the sign of mean sea level (MSL) pressure bias in ALADIN is "case" dependent so improvement in MSL pressure in Fig. 3.4 is thus relative and depends on whether we are in positive or negative "bias" situation.

Concerning the temperature in upper levels (Fig. 3.5), one can see relative improvement in 850 hPa but this positive change is not seen further in higher levels. On the contrary, we are experiencing increase of temperature bias from 700 hPa thus creating a vertical "dipole" in

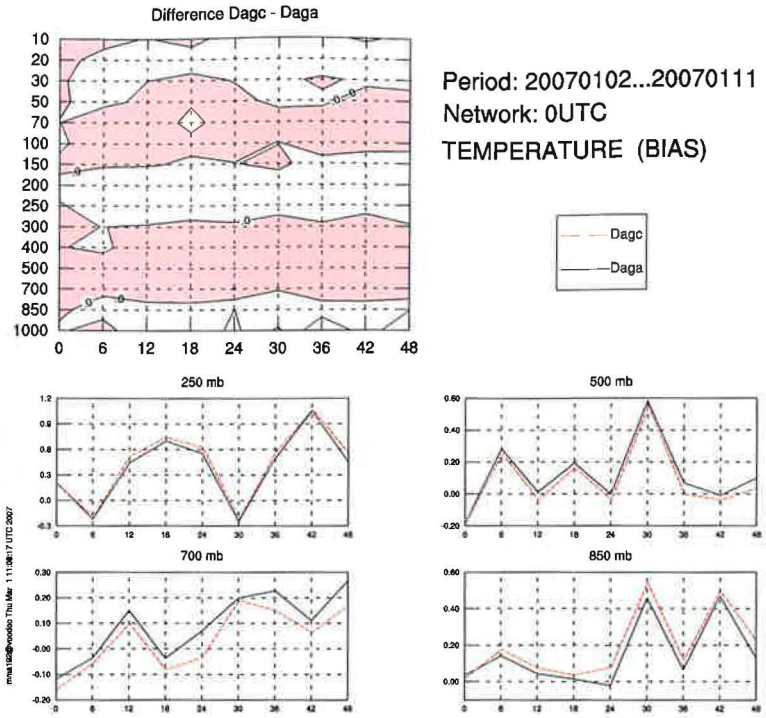

Figure 3.5: Scores of temperature for two versions of model ALADIN, one with envelope (red dashed line) and non-envelope (black solid line) within a ten day forecast period.

temperature between 850 and 700 hPa level. This can have several physical explanations. The first one could be that envelope orography enables higher vertical velocities at the windward sides of the slopes thus enhancing condensation of water vapor and precipitation rate. This could lead to warming of 850 hPa level due to latent heat release. As more vapor precipitates at lower layers there is a deficit of moisture at 700 hPa. This deficit can be responsible for the weakening of heat release in condensation process and finally also to relatively lower temperatures. Assuming that this Föhn effect is the main contributor to the temperature redistribution, one could try to apply modifications to the rate of precipitation introducing tuning constant that would control precipitation efficiency depending on the height of subgrid scale orography. Former version of precipitation scheme did not allow such changes, however, recent development of this scheme within ALARO-0 development concept enables even such flexible manipulations. The above idea was tested in ALADIN and validated using comparison of scores with respect to the reference operational run but without a very promising results as the sensitivity to the newly introduced tuning constant was negligible. The explanation of this quite surprising result is simply that all what could precipitate precipitated already in the single case. Then we are left only with a dry Föhn effect. Another mechanism responsible for the temperature problem can be related to the change of circulation which could produce large scale vertical motions and thus affects the temperature field. However, contribution of particular processes to the overall evolution of scores involves more complex investigation that is done in the next Section.

In the Fig. 3.6 the geopotential bias reveals similar "dipole" behavior as we could find in the temperature field with lower geopotential at 850 hPa and higher starting at 700 hPa indicating that the two phenomenons could be connected. As the last remark, a closer look at the pictures of vertical profile of bias evolution reveals some characteristics with semi diurnal period. This

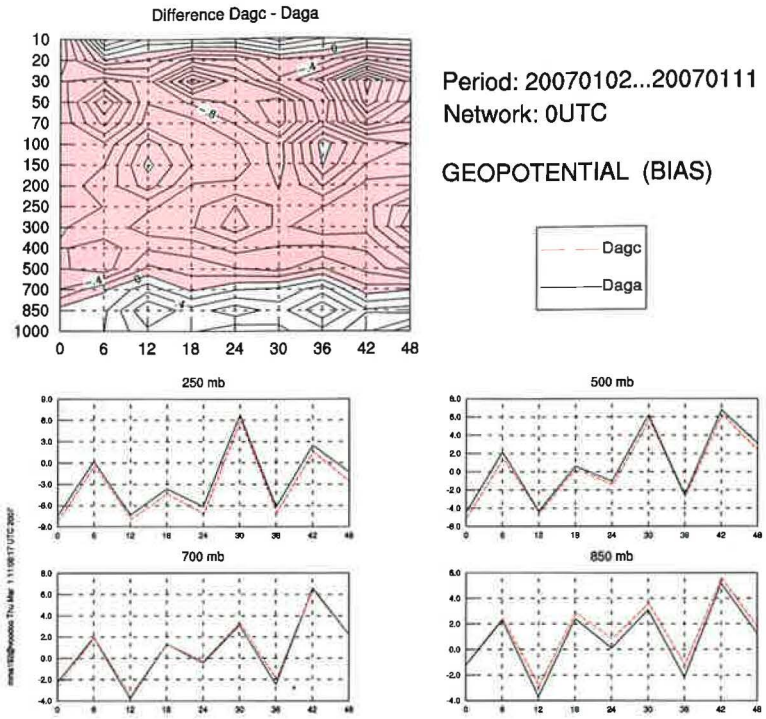

Figure 3.6: Scores of geopotential for envelope case (red dashed line) and non-envelope case (black solid line) within a ten day forecast period.

is actually the result of the different number of available measurements for verification in particular observing terms, especially soundings that are performed primarily in 12 hour cycle.

3.4.2 Geopotential differences

We have analysed differences in fields of temperature, wind and geopotential in two pressure levels, 850 hPa and 700 hPa for 24h forecast range. The investigated 10-day period (02-11/01/2007) was chosen to be a representative one with mainly zonal flow with high as well as low wind speed situations which is appropriate for studying of the effects of drag. The average flow in both pressure levels can be found in Fig. 3.7. It is not surprising that while in 850 hPa the flow is almost completely blocked and separated in region of the Alps, in 700 hPa we have more cross-mountain flow.

Let's fist analyse a differential geopotential field at 850 hPa. We can clearly see that leaving envelope orography and substituting with a new drag brings some mass redistribution. One can distinguish two main effects here. The first one is the dynamic effect of flow blocking by mountain ranges. That is the case primarily of the Alps and the Carpathians Mountains where with envelope we see relative elevation of geopotential at the wind ward side and a sharp drop at the lee side. Similar behavior is known from hydrostatic theory of flow response to the obstacle. Apparently, this dipole is exaggerated at the Alps region, which is mainly the result of extrapolation in post processing from hybrid to pressure coordinates. One should also note that 850 hPa level is almost completely covered by mountains masses in the region

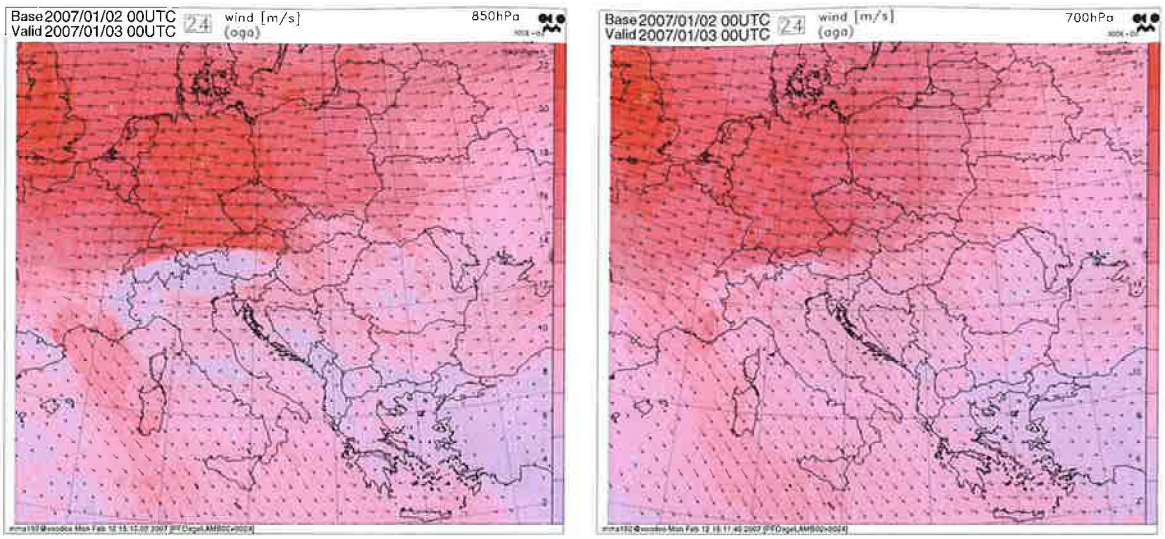

Figure 3.7: Mean wind field at 850 hPa and 700 hPa level for period 2-11/1/2007 for non-envelope version of ALADIN model.

of the Alps. Closer look at the Fig. 3.8 reveals that area of increased geopotential due to blocking of the Carpathians Mountains is larger than the one of the Alps despite the fact of lower orography variance values (see Fig. 2.2). The explanation could be that the Carpathians, with its characteristic bending and more perpendicular orientation with respect to the zonal flow, are disposing with higher potential for the large scale flow blocking than the Alps. As for the second effect, this one impacts larger scales and is related to the depression behind the mountain ranges after new drag scheme was established. At the first glance, we are getting a contradiction between these two effects. On one hand, envelope orography increases flow blocking at the wind ward sides, so one would expect that there will be more flow going around the obstacle thus causing a lower geopotential behind, but on the contrary, the geopotential is actually greater, which is not expected. However, one must realize, that the effect of flow blocking is also to increase cross mountain pressure gradient leading to the enhanced cross mountain flow and thus, simply said, transporting more mass behind. At 700 hPa we are primarily left with two centers of depression behind the Alps and the Carpathians with some mass accumulation mainly at the lower border of the integration area as a consequence of mass redistribution. However, we can still find a dynamical hydrostatic drop of geopotential over the Alpine ranges, but no more over the Carpathians as they are not sufficiently high to affect the geopotential at this level. Apparently, geopotential difference fields resulting from envelope removal and implementation of new drag scheme are approaching the scale of Rossby radius of deformation (sub-synoptic scale), thus one should take into account a geostrophic equilibrium here. Indeed, when examining the differential wind fields (Fig. 3.8), one can find a cyclonic vortexes associated with the geopotential deformations.

3.4.3 Temperature differences

In the following, we will investigate the distribution of temperature differential field. We can recognize again the dynamic effect of mountain ranges. It is evident, that envelope orography forces stronger upward motions leading to cooling at the wind-ward side and warming at the

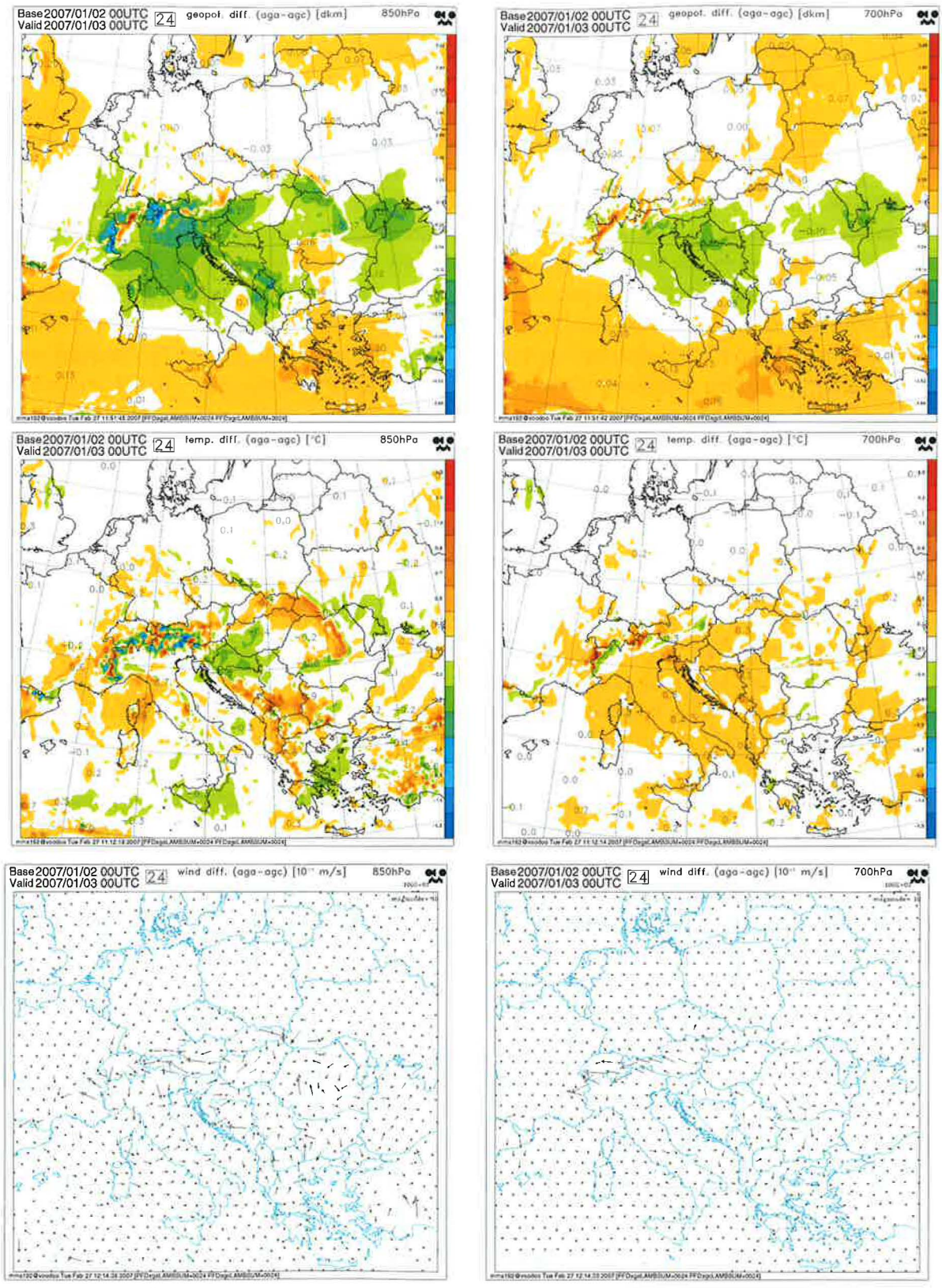

Figure 3.8: Differential fields of geopotential, temperature and wind (top middle and bottom panel respectively) for 850 hPa and 700 hPa levels (left and right panel) between version using no envelope and present scheme (aga) and version with envelope using former scheme (agc).

lee side of the mountains. This pattern can be clearly seen at 850 hPa for the Carpathians and 700 hPa for the Alps. However, this is not very surprising. More interestingly, 850 hPa level reveals some curious circular temperature patterns with opposite sign. Warm anomaly behind the western and cold anomaly behind the eastern part of the Alps. These two areas correspond to smaller vorticity maximums embedded within a large depression behind the Alps and are forced by a shear effect. When looking at the layout of western vortex, we can see that it is well pronounced at 850 hPa while at 700 hPa we can hardly recognize any cyclonic circulation. Thus we are experiencing weakening cyclonic vortex with warm core which is in accordance with equation of thermal wind balance. The second vortex is also cyclonic, but this time with cold core so one would assume that this one is intensifying with height. Indeed, differential wind field confirms our assumption. The cyclonic vortex behind the eastern Alps is more pronounced at 700 hPa then 850 hPa. All that proves that our model is really internally consistent. Finally, temperature field at 700 hPa evidently possesses positive anomaly that is consequence of weakening large scale depression behind the Alpine region.

As the conclusion of the above analysis, we can see that removing the envelope has several dynamical effects. It reduces the vertical velocities associated to the passage of the flow over the obstacles thus locally diminishing temperature perturbations at the wind ward and lee sides of the hills. This effect is quite straightforward and it is obviously the result of lower mean orography hight. Another effects are more interesting as they have larger scale impact redistributing mass and subsequently initiating geostrophicaly balanced circulation. Lee cyclonic vortexes are formed with decaying intensity with hight forcing existence of warm core at 700 hPa and so negatively effecting temperature bias as could be seen in Fig. 3.5. This results from exaggerating the amount of drag within subgrid scale orography height thus supporting the flow separation rather then enabling it to pass over. The problem is that this kind of flow blocking due to form-drag is not equivalent to flow blocking due to resolved orography. While the blocking effect of envelope is controlled explicitly by the dynamical part of the model standing on the right hand side of momentum equations, our parametrisation acts only locally and does not possess with 3D response which cannot be obtained with the concept of single column computations as is the case of our scheme (see Chap. 2). The lack of this 3D behavior could to be responsible for insufficient representation of geopotential hight elevation on the wind-ward portion of the mountains and thus underestimation of the cross-mountain pressure gradient.

3.4.4 Precipitation field

Overestimating of precipitation at the mountain areas is already well known problem of the envelope orography. The aim of this Section is double: (i) to verify the impact of envelope removal to distribution of precipitation (ii) to diagnose the significance of potential influence of latent heat release to temperature anomalies.

Before we start to analyse differences of precipitation intensity between two versions of model ALADIN (with and without envelope), it is important at first to get a picture of the layout of total average precipitation inside our integration area. As we are no more diagnosing a continuous field now, we have to know where exactly does the differencing make sense (subtracting two zero's contains no valuable information). We can see in Fig. 3.9(a) that

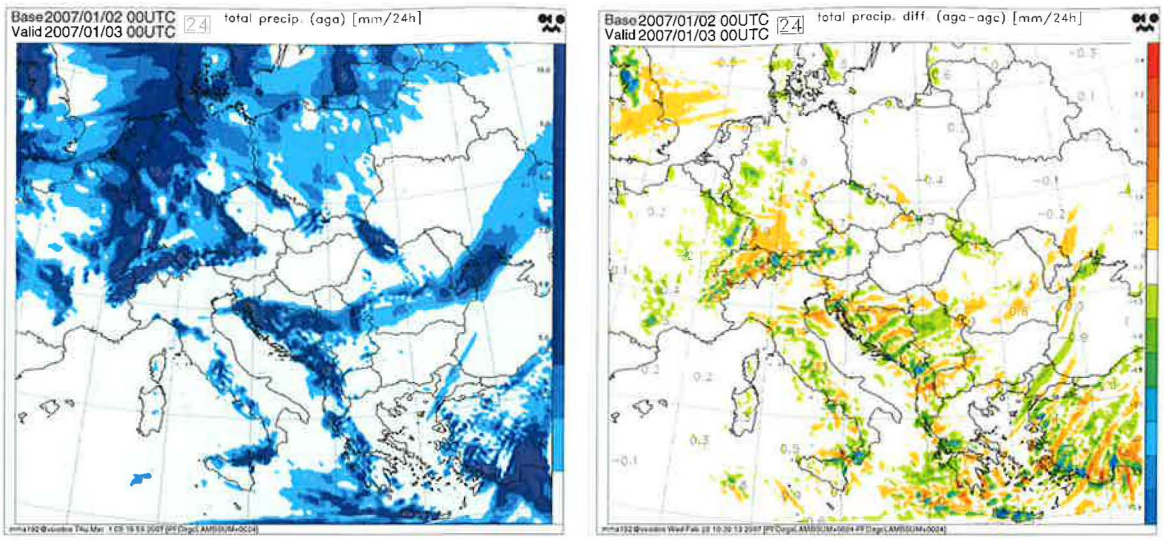

(a) (b)

Figure 3.9: (a) average rate of total precipitation after the first 24h of integration without envelope orography for 10-day period 02-11/01/2007. (b) difference of total precipitation rate between non-envelope and envelope version of ALADIN

most of the precipitation activity is situated at the flat areas which is not optimal for our study.

More intense precipitation event at the mountain areas would suite our problem much better. However, we have quite intense precipitations at the northern Alpine cape and British mountains. At this two regions, the interpretation of the impact of envelope removal is quite straightforward. When looking at the deviations in precipitation with respect to envelope, we can see that precipitation shows some relative decrease at mountain peaks, or alternatively, places with highest value of standard orography deviation. Consequently, more moisture is advected to the lee of the mountains where the residual moisture precipitates. It's hard to interpret the rest of differential precipitation field at for us interesting areas as we have either precipitation in very complex terrain or the field of average precipitation is not very homogeneous. However, we can generally observe some common behavior, specifically a rapid decrease of precipitation rate at mountain peaks. Although the examined period does not possess ideal configuration of precipitation field with respect to the orography it reveals some characteristics which are in agreement with already well known envelope problem.

Further, we will touch a relation of the change of precipitation to the temperature deviations to test our assumption of Föhn effect and its influence on temperature bias "dipole" behavior. Comparing Fig. 3.9 to temperature differential field Fig. 3.8, one can see that there is not much "correlation" between precipitation and temperature deviations. Thus one can conclude that the change in precipitaion does not participate in our temperature problem, at least for this period. However, it does not exclude a possibility that there can be a case at which the latent heat release in very intense precipitation events can considerably influence temperature layout.

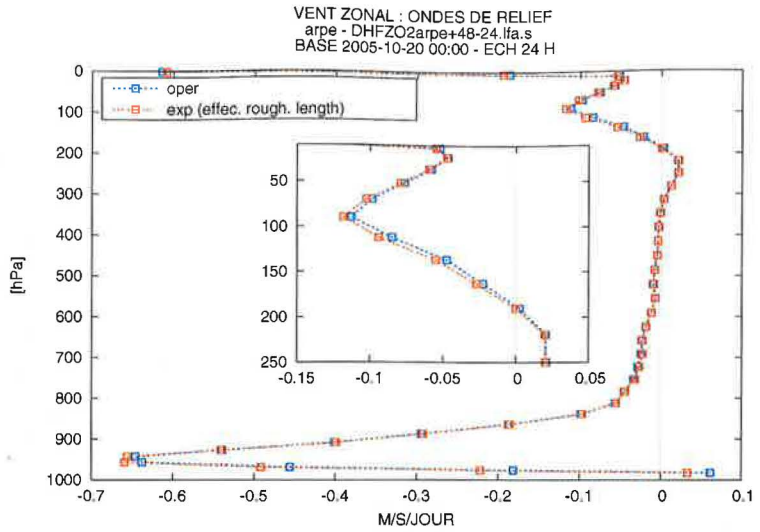

Figure 3.10: Comparison of two vertical profiles of GWD scheme induced drag for the case with reference value of roughness length (blue) and with modification preventing it to exceed value 1 m (orange).

3.5 Interaction with effective roughness length

The turbulent drag exerted by a subgrid obstacles is out of gravity wave drag and form-drag another important contributor to the total surface drag in large scale models. In addition to the vertical flux of horizontal momentum generated by gravity waves, there also exists a momentum flux due to turbulent eddies. Clearly, they are not resolved by the model and therefore need to be parametrised. In ALADIN/ARPEGE NWP model, the concept of *effective roughness length* is used. This approach is well justified by observations of logarithmic wind profiles and led to a significant improvement in the performance of a number of NWP models. However, the concept has a number of disadvantages. In some areas the roughness length can be enhanced well enough to negatively affect low level wind speeds. Besides, there are still difficulties in understanding the interactions with stability as well as with gravity wave drag and flow-blocking schemes. In a view of these concerns, it is reasonable to put some attention to this problem. The aim of this Section is not to propose a new parametrisation scheme for sub-grid scale turbulent drag, but to try to diagnose the sensitivity of form drag to the value of roughness length.

In order to examine the impact of roughness length, we have introduced simple modification to the code that prevents the roughness length z_0 to exceed the value of 1 m. This way we suppress the total amount of surface turbulent drag thus allowing higher surface wind speeds. Apparently, such modification is not physically consistent and cannot be integrated into operational usage. Our intention is to examine the response of GWD drag scheme to change in z_0 and test the suspicion that turbulent drag "eats" too much wind speed thus lowering the form-drag. The new setting of effective roughness length has been tested using global model ARPEGE. On Fig. 3.10 we can see that there is a minor increase of drag at lower as well as upper levels however, the overall impact of reduction of roughness length is really negligible. Thus one may conclude that there is actually not much interaction between

the two features.

3.6 Lift effect on turbulent drag

As we could see in Sec. 2.3.9, the effect of lift is not only to change direction of the wind, but it also amounts to increase the total drag by f'/f proportion within the height $\mathcal{H}$ above the ground. In the previous formulation of the lift parametrisation, the turbulent and convective friction terms were assumed to be negligible compared to the mountain drag ones at places where the lift was active. But this assumption might not be well fulfilled at all cases. For instance, if there exists a relatively thin layer with low stability adjacent to the ground, this would lead to turbulent mixing. Thus contribution of divergence of turbulent flux has to be accounted in establishing geostrophic equilibrium at places where the lift exists, and should be corrected in the same manner as mountain drag and Coriolis force by coefficient f'/f. On average, the role of vertical turbulent flux of horizontal momentum is to accelerate the flow at the lowest layers and decelerate it at the top of boundary layer, which is obviously the consequence of baroclinicity. One could expect that adding some additional portion of turbulent flux should lead to a relative increase of wind speed at the surface. This proposal has been tested modifying ARPEGE/ALADIN GWD parametrisation scheme. Because of some complicating programing issues, f'/f proportional increment of vertical turbulent flux has been superposed on top of gravity wave one rather then turbulent flux itself, but clearly this bypass does not change the resulting physical effect. We can then schematically write

$$\tau = \tau_w + \tau_f \left(1 + \frac{f'}{f}\right) + \tau_{tur} \frac{f'}{f} \,.$$

However, one has to be cautious when implementing the superposition of these two different fluxes. The reason originates from the numerical security algorithm that is applied to the final fluxes at the end of GWD drag routine (see Sec. 2.3.11). This numerical security protects the solution from nonlinear instability. However, we have experienced problems when adding of these two fluxes have been performed before application of numerical security algorithm. Indeed, while the drag due to divergence of turbulent flux is always parallel (but opposite) to the mean flow acting exactly against it, the gravity wave drag can have generally different direction with respect to the mean flow due to anisotropy of the subgrid mountains. So each of these two fluxes have to be treated separately.

The impact of this modification was tested by 48h integration of global model ARPEGE. In Fig. 3.11 we can see 24h tendency of zonal wind due to superposition of divergence of vertical flux induced by GWD drag parametrisation and f'/f proportion of turbulent flux.

As one can see, the resulting effect is indeed reduction of drag close to the surface however, only the lowest model levels are influenced by this modification without any sign of relative increase in form-drag at the upper part of boundary layer as one would expect. Moreover, turbulent and dynamical tendencies seem to adapt to the applied modification accordingly resulting in very small impact on the overall mean tendency of zonal wind. Nevertheless, this does not necessarily mean that the impact on the prognostic variables will be negligible. We

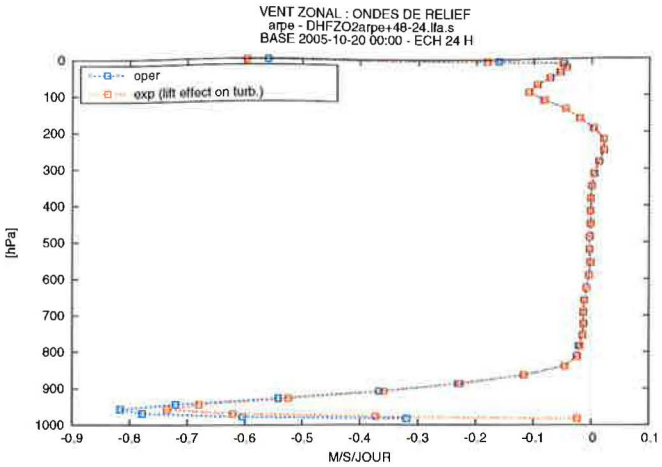

Figure 3.11: Contribution of f'/f proportion of turbulent flux of horizontal momentum due to lift effect in geostrophically balanced flow. The resulting increment of turbulent flux is superposed on top of the gravity wave one.

have made the analysis of the contribution of particular constituents to the overall tendency in order to verify consistency of implemented changes with physical preconditions and backtrace possible errors, though internal feedbacks stay hidden anyway. In the following, we will aim our concentration to the impact of above proposed modification to the quality of the forecast. For this purpose, we have computed objective scores for single 48h forecast with ALADIN. Although from the statistical point of view using only one model run for verification is not very reliable solution, it can provide useful information and potentially reveal strong signal at low computational cost. The results can be seen in Fig. 3.12.

Scores of temperature and MSL pressure seem to be unaffected by our change, but one can clearly note a considerable distortion of surface wind in both bias and RMSE. The negative results we have obtained were quite surprising because we assumed that the implemented modification will result in more realistic description of the lift effect. The situation did not improved event when we tried to subtract a βS portion of the resulting turbulent flux increment in order to account for the valley air isolation.

The source of the problem could be hidden in a partly contradicting aspect of difference between the concept of the low level averaging leading to the effective surface values and unmodified actual profiles used to calculate turbulent fluxes. Therefore, it is questionable if the combination of the two can work together.

3.7 Retuning ARPEGE/ALADIN GWD scheme

As could be seen, comparing the objective scores of surface wind for operational version of model ALADIN and parallel suite with envelope, the present drag parametrisation does not sufficiently substitute the effect of envelope having negative bias in the surface wind and temperature. This led to the conclusion that our parametrisation exerts too much drag within subgrid mountain depth levels decelerating the low level flow and reducing the turbulent mixing.

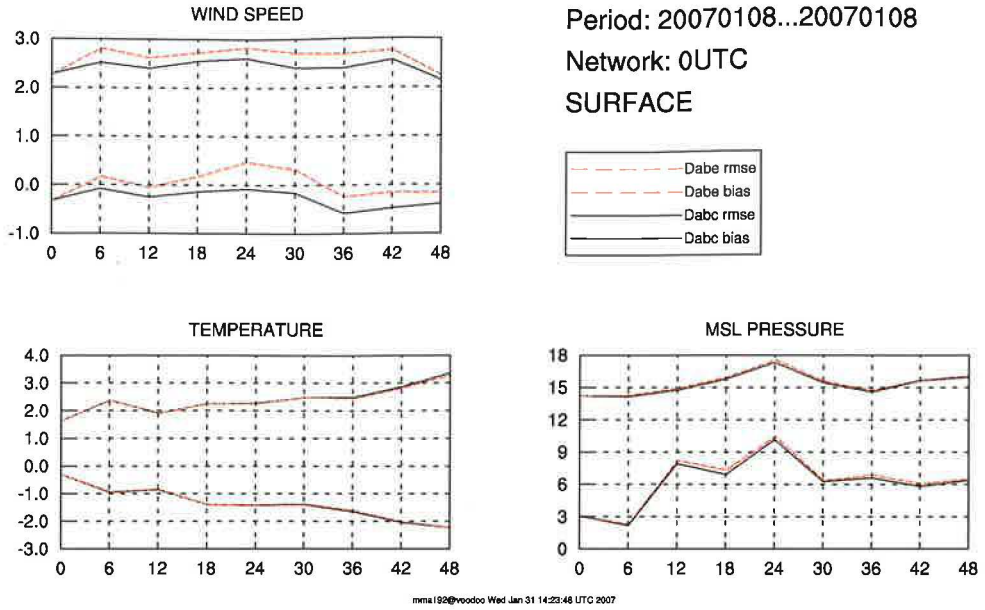

Figure 3.12: Evolution scores for reference run (black solid line) and modified version (red dashed line) taking into account the lift effect on turbulent drag for a single 48h forecast. Lower lines represent bias and upper lines RMSE of corresponding quantities.

As the most straightforward approach how one can try to eliminate this negative behavior near the surface is to retune the current scheme to obtain the lower values of the form-drag. This relatively simple task has to be done with care, because we do not want to touch stratospheric wave-deposition rate which is generally considered to be an appropriate one. This condition actually simplifies the tuning process because it reduces the number of freedom of the problem. For the mountain and stratospheric terms, one can schematically write

$$\text{stratosp. wave drag} = f(\kappa, U_s, F_c/F) \tag{3.1}$$

$$\text{mountain drag} = f(C_d, \kappa, F_c/F, L_t) \tag{3.2}$$

In the mountain depth level, the drag is mainly controlled by two constants C_d and κ, while in the stratospheric part it is κ and surface wind U_s. In order to reduce the surface drag we have to tune C_d down. However, this will lead to increase in surface wind followed by enhanced vertical flux of horizontal momentum thus enhancing also the upper wave deposition. To keep the stratospheric part unchanged, we have to tune κ towards lower values. In the previous formulation of the scheme, the values of C_d and κ were respectively 5.4 and 0.02. We have tried to set C_d to its theoretical value of 2.0 and determine corresponding κ for which the stratospheric deposition rate would resemble the operational one. Several tunings have been tested and as one can see on the Fig. 3.13 the best fit with former stratospheric wave drag is achieved for $\kappa = 0.012$. Having these two consistent tunings (reference one and new one) enables us to make a linear extrapolation of our controlling constants. Of course, one cannot a priori assume linear dependency here, but it shows that for this range of values the linear dependency is roughly fulfilled. Thus we can change the amount of form-drag while preserving the well validated stratospheric deposition rate. However, this is true only when assuming that we do not modify any part of internal physics in our scheme. If we do so, the new setting has to be validated and possibly retuned again in order to satisfy the stratospheric constraint.

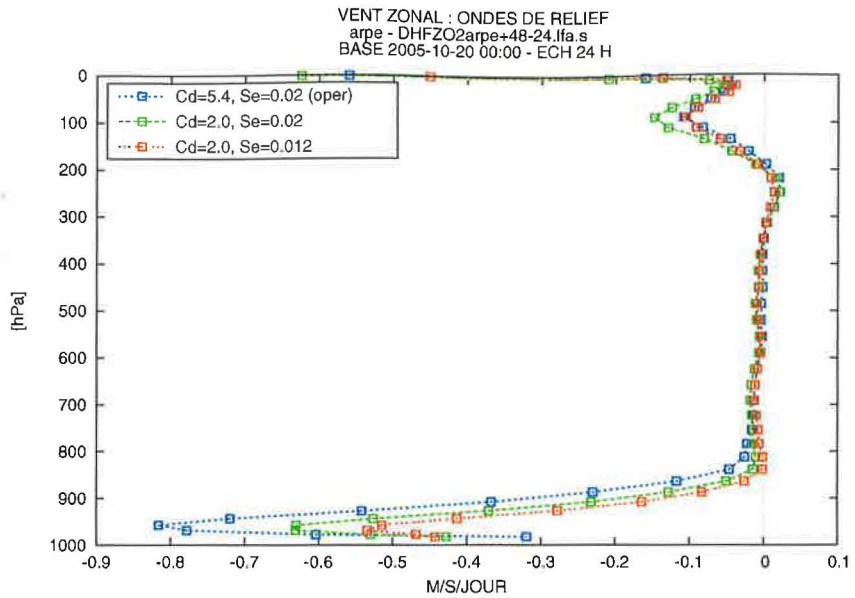

Figure 3.13: Drag exerted by GWD parametrisations on the zonal wind for several settings of coefficients Cd, and κ.

3.8 Validation of the new tuning

In the Sec. 3.4 we have introduced a detailed analysis of the effects of the envelope suppression from two different angles of view: objective scores and horizontal distribution of differences for several prognostic quantities, which gave us better insight to the problematics. We have concluded, that at present state, the parametrisation is exerting too much drag within subgrid scale mountain heights thus influencing not only low-level flow (underestimating the surface wind speed) but also the large-scale circulation which is cumbersome to reproduce as we can not control it directly. Furthermore, in Sec. 3.7 we have discussed some issues around tuning procedure. Under the constraint of preserved stratospheric wave deposition we could extrapolate linear dependence of two controlling constants Cd and κ. Linking it together, one can propose relatively simple solution to the above mentioned problems, and that is, to retune the scheme reducing the total amount of the form-drag. The main objective of this Section will be to diagnose the effects of form-drag reduction and potentially propose and validate a new, more appropriate tuning.

Knowing that previous tuning of $C_d = 5.4$ overestimated the magnitude of the form-drag, setting C_d to its theoretical value 2 was supposed to be a good starting point for further testing. The corresponding value of κ (that preserves the stratospheric deposition rate) is 0.012 (see Sec. 3.7). The resulting impact of the new tuning on the objective scores for the period 02-11/02/2007 can be found in Fig. 3.15 giving promising results with improvement in surface wind velocity as well as some minor improvement in surface temperature, though it is still not sufficient when compared to envelope effect. MSL pressure and geopotential are systematically shifted towards lower values which shows to bring relative improvement in bias for this particular investigated period. However, as mentioned earlier, the result is not always positive and is "case" dependent. Indeed, this was confirmed on the scores of parallel test from different period 24-31/01/2007 which was the situation of large baroclinic instability over

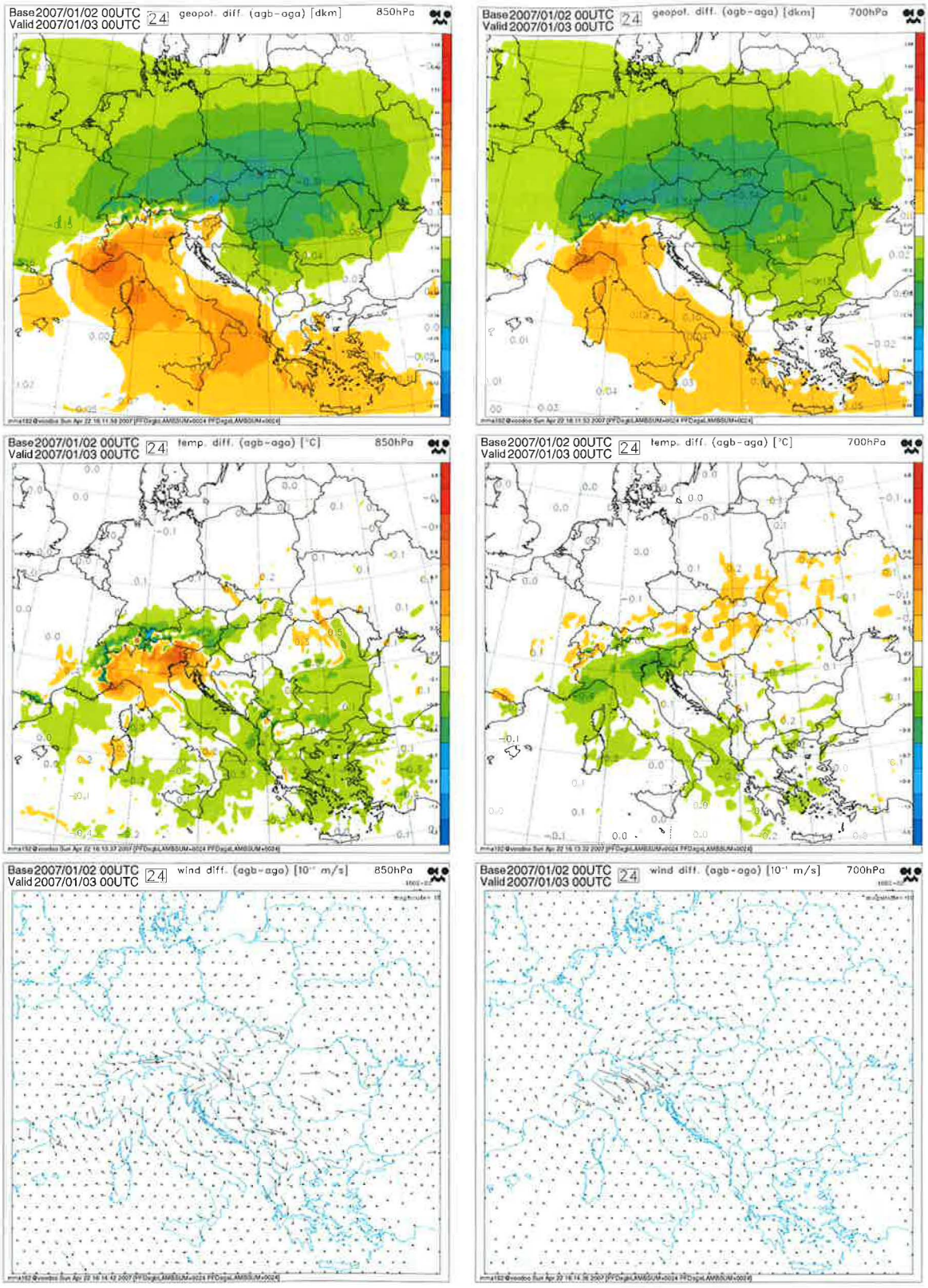

Figure 3.14: Differential fields of geopotential, temperature and wind (top middle and bottom panel respectively) for 850 hPa and 700 hPa levels (left, right panel) between version with reference setting $C_d = 5.4$, $\kappa = 0.02$ (aga) and parallel suite with new tuning $C_d = 2$, $\kappa = 0.012$ (agb).

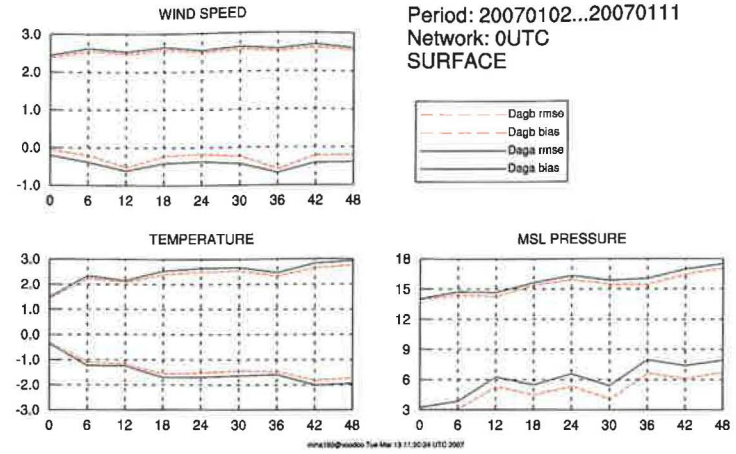
WIND SPEED
Period: 20070102...20070111
Network: 0UTC
SURFACE
Dagb rmse
Dagb bias
Daga rmse
Daga bias
TEMPERATURE
MSL PRESSURE

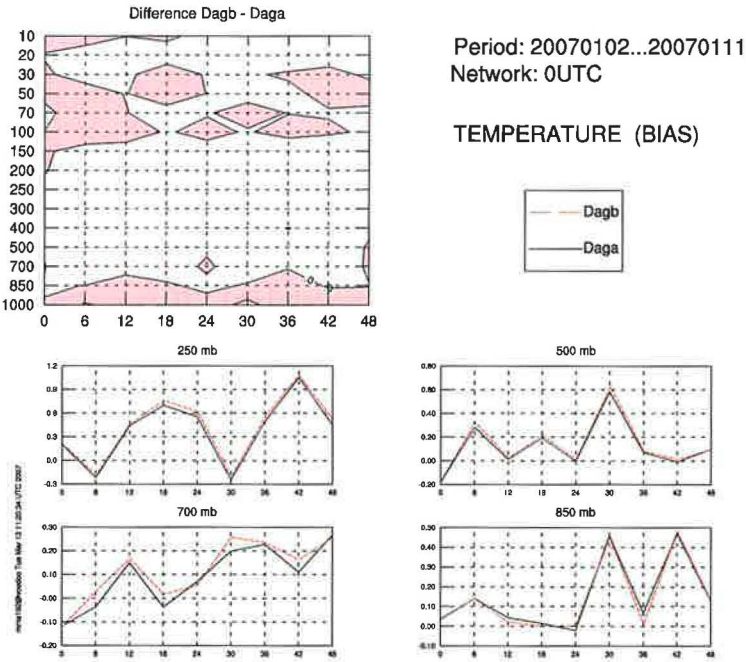
Difference Dagb - Daga
Period: 20070102...20070111
Network: 0UTC
TEMPERATURE (BIAS)
Dagb
Daga
250 mb
500 mb
700 mb
850 mb

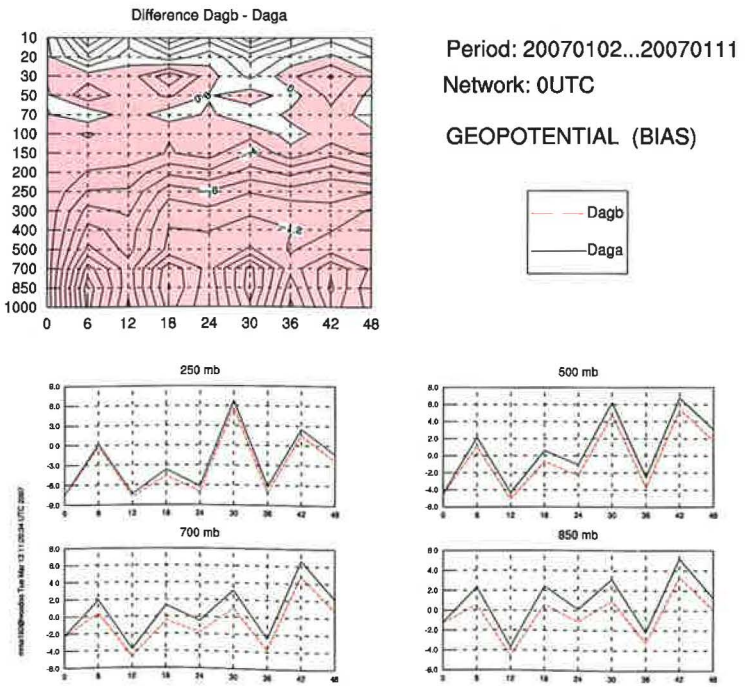
Difference Dagb - Daga
Period: 20070102...20070111
Network: 0UTC
GEOPOTENTIAL (BIAS)
Dagb
Daga
250 mb
500 mb
700 mb
850 mb

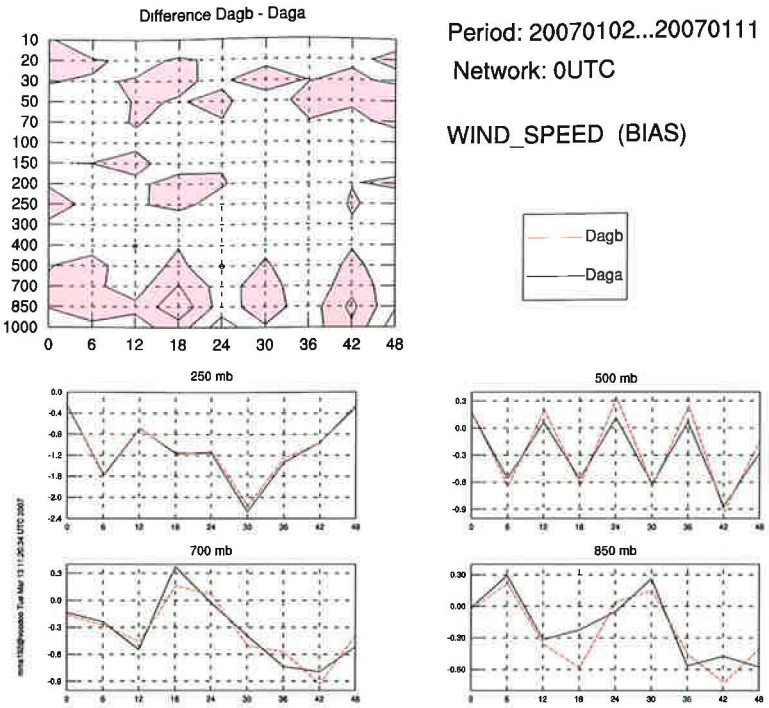

Figure 3.15: Comparison of scores for surface variables, temperature, geopotential and wind for new tuning $C_d = 2$, $\kappa = 0.012$ (red dashed line) and reference operational setting $C_d = 5$ and $\kappa = 0.012$ (black solid line).

the Europe with strong wind speeds. In this period we get similar results for scores of wind and temperature, but this time with relative deterioration of MSL and geopotential. Apparently, the evolution of geopotential is determined also by other "uncontrolled" mechanisms resulting in negative bias in strong wind situations and vice versa. Nevertheless, the RMSE for both cases is higher which is not a good indication.

In Sec. 3.4 the analysis of differential fields was introduced in order to examine the effect of envelope suppression on some prognostic variables. In the following, we will perform similar analysis but this time with the view of better understanding of the impact of form-drag reduction comparing the 24h forecasts of NWP model ALADIN with two settings of the GWD scheme: the reference operational one (with $C_d = 5.4$, $\kappa = 0.02$) and one with the new tuning (with $C_d = 2$, $\kappa = 0.012$). As can be seen in Fig. 3.14 reduction of drag leads to a relative acceleration of the flow especially over the Alps with evident Föhn effect enhancement. Nevertheless, one cannot overlook a noticeable mass redistribution induced by the Alpine region, which is however not exactly in "phase" with the effect of envelope (see Fig. 3.8).

This leads to the conclusion, that at present state, retuning of the GWD scheme can partly substitute the envelope in the means of improvement in the prediction of surface variables, nevertheless, it is not able to sufficiently substitute the directional aspects with respect to the forcing of envelope, resulting in the geopotential distortion. Thus one can propose as a solution to tune C_d somewhere between the former value and the one suggested above to still benefit from the positive impact on the surface wind and temperature and at the same time to not distort the geopotential too much. After several experiments, setting with

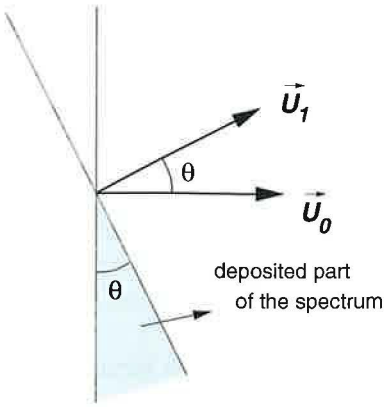

Figure 3.16: The part of the deposited spectrum (light gray) when the wind at the surface and at the level above has different directions.

$C_d = 3.5$ and $\kappa = 0.016$ showed to be a reasonable compromise between the two giving the acceptable results. Still, it cannot be considered as a definite solution which means that further improvement of the scheme will probably involve accounting for some additional presently missing effect.

3.9 Multi-directional aspects

As we could see in the previous results, retuning of our scheme improves the situation a bit but not sufficiently because the direction of the correction is not the same one as what had to be compensated for. This inconsistency is responsible for the geopotential distortion and temperature problem at higher levels. Questioning the "angle" repartition, one may look in direction of the work of Catry (2005) on spectral momentum deposition, who has already developed the corresponding modifications to the code. In the following, we will introduce a short description of this method and in the latter, we will make a validation comparing the scores against reference operational version of ALADIN model.

The resulting linear drag induced by elliptic mountain with aspect ration γ and direction ψ, developed by Phillips (1984), has been already presented in compact notation by (2.11). The part of this equation which depends on γ and ψ is actually an analytical solution of equation (again in compact form)

$$\vec{D} = \int_{-\pi/2}^{\pi/2} [A_1, A_2] d\varphi \tag{3.3}$$

where φ is the angle measured counterclockwise with respect to the reference direction given by wind vector and A_1, A_2 functions of γ, ψ and φ (see Appendix of SMF00). The integration is performed over the range enclosing the left and right quadrant of the wind vector thus giving an angular spectrum of momentum flux directions. In ALADIN/ARPEGE GWD parametrisation scheme an uni-directional representation of momentum flux is used, i.e. one first computes the surface momentum flux vector and then traces the changes of this single vector throughout the upward propagation of the momentum flux in order to keep the computational cost low. However, the stress vector should be recomputed at each level integrating over a corresponding

spectrum of directions. The main difference between the two approaches (uni- and multi-directional) is evident when taking into account the change of the wind direction with height as the part of the spectrum may become orthogonal to the wind at higher level and hence is deposited and unable to contribute to the momentum flux at higher levels (see Fig. 3.17). Consequently, the boundaries of the integral (3.3) are reduced. Hence, the direction of the stress at arbitrary level, evaluated integrating (3.3) within the corresponding spectral range, can be generally different from the one at the surface. More detailed description is out of the scope of this work and can be find in Catry (2005).

The general impact of the multi-directional modification is to reduce the amount of form-drag resulting in higher wind speeds near the ground as can be clearly seen on the wind speed over the Alps in Fig 3.20. Consequently, the scores for all surface prognostic quantities have improved considerably with respect to the reference operational version. Especially the scores of surface wind speed are now approaching that of envelope orography (see Fig. 3.18). However, the positive impact is localised only in the lower layers and doesn't extend higher up. Concerning the wind, except of the surface, it is relatively smaller with most pronounced maximums of deceleration (with respect to the reference model) in 850 hPa and 200 hPa. Nevertheless, the most interesting part happens in the vertical layout of geopotential. In Fig. 3.18 one can not overlook the switch between the systematically lower geopotential in the troposphere and higher values in the stratosphere indicating that there might be some problems in the representation of stratospheric deposition. Indeed, this was confirmed by diagnosing the vertical profile of global mean 24h-tendency of zonal wind due to contribution of particular effects (including GWD one). It shows (see Fig. 3.17) that the stratospheric deposition rate is extremely overestimated decelerating the flow at higher levels. Resulting gravity wave drag is sufficiently large to induce a mass redistribution in stratosphere. In order to reduce the wave-drag, one could suggest retuning the κ towards the lower values, however, one can see that apart from the exaggerated stratospheric deposition rate, the lower part of the drag shows some "strange" behaviour too. We can see that drag at the lowest model level due to our scheme started a positive feedback of turbulence contribution to the mean wind tendency which could be responsible for the better score of temperature and wind at the surface.

As the above tested multi-directional feature is not giving a good results, although Catry (2005) showed a positive impacts on the scores in the ARPEGE, it can not be thus implemented operationally. However, presenting this negative result here is useful from the two aspects: it shows the advantage of using several diagnosing and verification tools paralelly to obtaining a better analysis of the overall behaviour of the scheme and secondly, it shows the sensitivity of the response of the flow to the representation of the sub-grid scale orography effects. Unfortunately, we could not further investigate the reasons of failure of our attempt to integrate a multi-directional feature into the ALADIN CHMI framework (mainly because of the time issues), but this does not mean that further efforts could not bring a satisfactory results similar to the ones of Catry (2005).

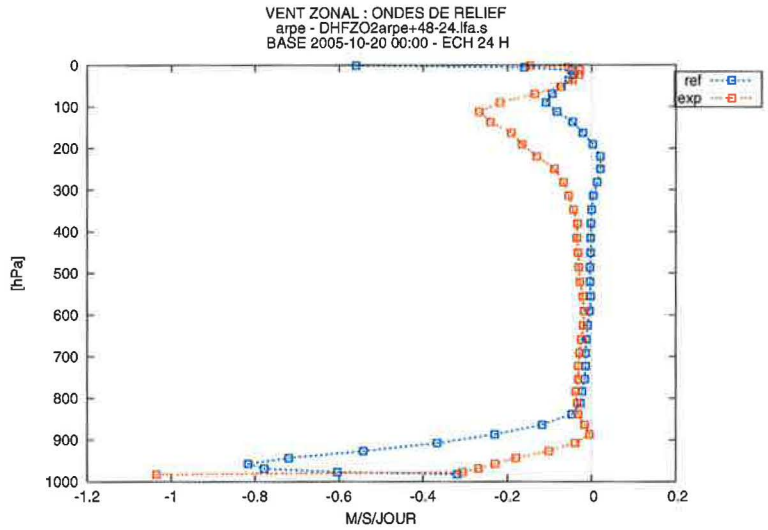

Figure 3.17: Vertical profile of drag induced by GWD parametrisation including multi-directional modification (orange) with respect to the reference operational version of the scheme (blue).

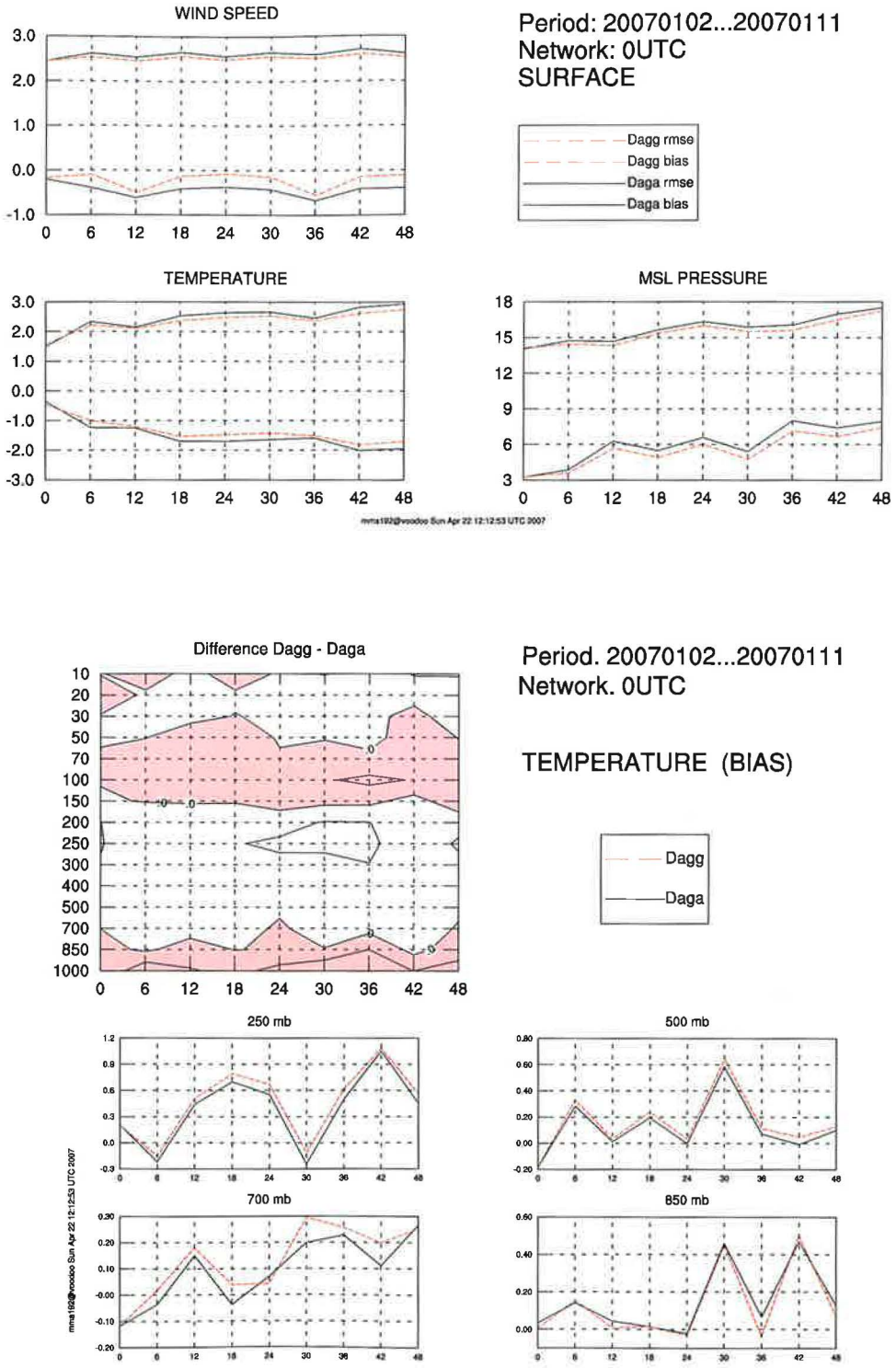

Figure 3.18: Comparison of scores for surface variables (top) and temperature (bottom) for multi-directional modification (red dashed line) and reference uni-directional operational scheme (black solid line).

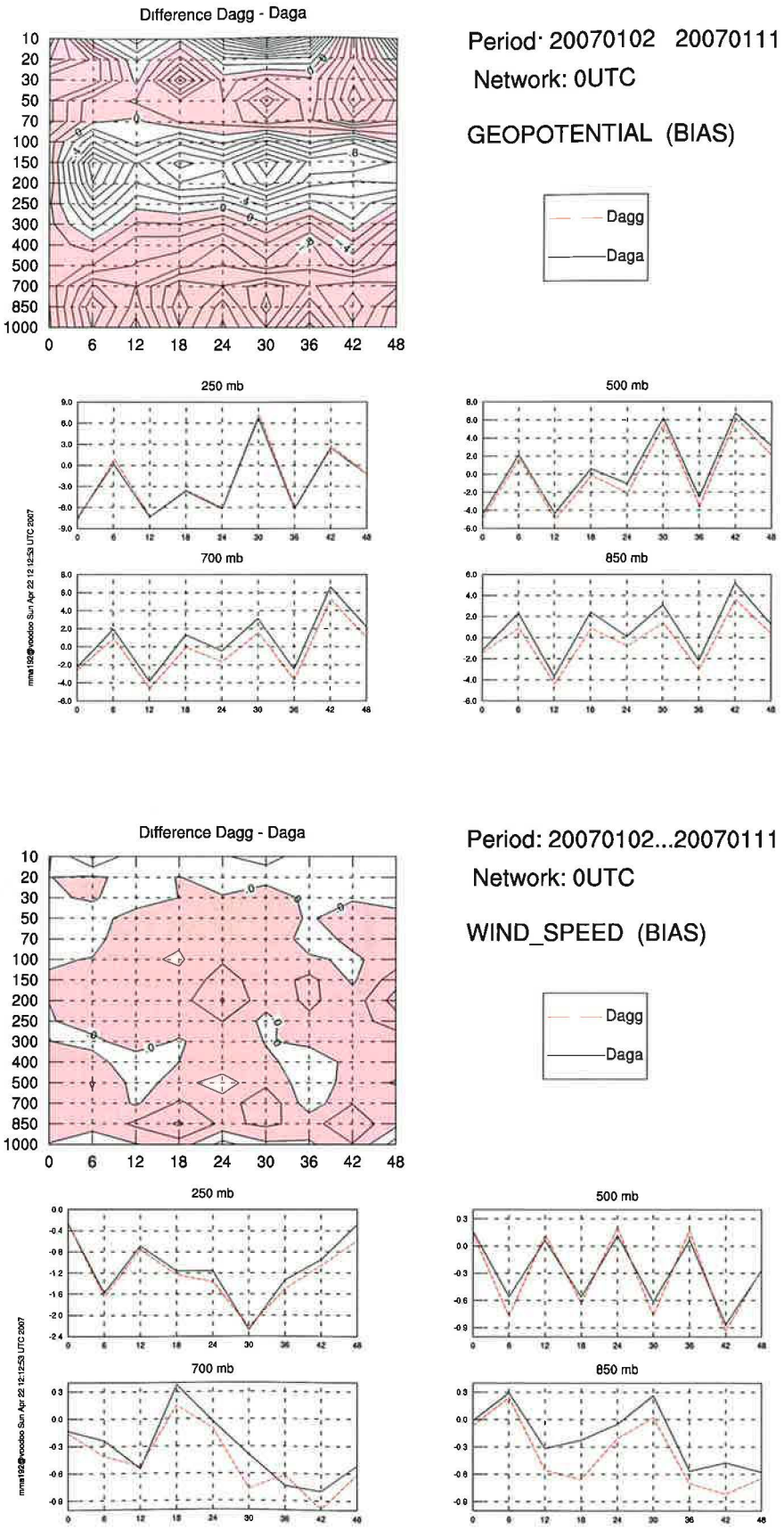

Figure 3.19: Comparison of scores for geopotential (top) and wind speed (bottom) for multi-directional modification (red dashed line) and reference uni-directional operational scheme (black solid line).

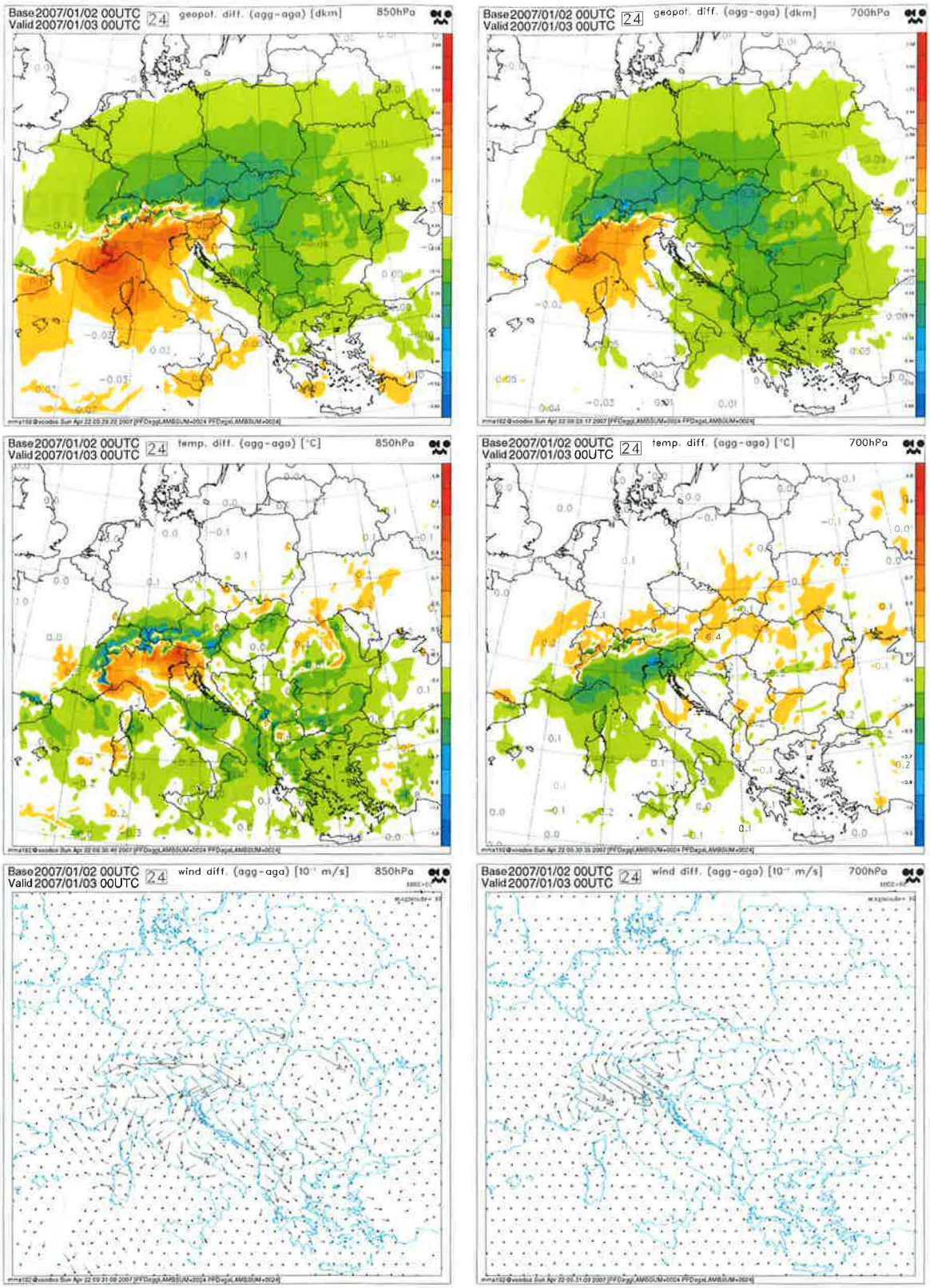

Figure 3.20: Differential fields of geopotential, temperature and wind (top middle and bottom panel respectively) for 850 hPa and 700 hPa levels (left and right panel). Difference is taken between the version including the multi-directional modification (agg) and operational version with reference settings (aga).

Conclusion

Parametrisations of sub-grid scale orography effects are presently widely used by many operational NWP models. We have outlined their importance for the continuous improvement of the quality of numerical weather prediction and climate forecasts. The latest version of ALADIN/ARPEGE GWD parametrisation scheme was described to present the whole spectrum of the processes involved.

Complementary diagnostic tools for particular experiments have been developed which can be further used for similar tests. The validation of new modifications was done in two prediction scales (limited area and global) and three different approaches were used to analyse the obtained results: the study of vertical drag profiles, verification of objective scores and differential fields of prognostic variables between the two model versions.

The detailed analysis of the effects of envelope suppression was presented leading to a conclusion that the envelope removal not only has a negative impact on the scores of surface quantities, but also deteriorates the geopotential field due to mass redistribution as the directional forcing of a new parametrisation is not equivalent to that of envelope. Consequently, the associated geostrophically balanced circulation induces temperature anomalies at higher levels. Based on this results, it was concluded that present scheme is exerting too much drag at low levels.

Integration of turbulent drag into lift mechanism has been implemented to obtain, from the theoretical point of view, a more realistic representation of the lift effect. However, this modification did not have a positive feedback on the resulting scores. In the next step, a new tuning of the scheme have been proposed reducing the form-drag part of the total drag. The new setting have partially improved the situation, especially for the surface quantities, however the problem with the geopotential still remained as the correction is not the same as what have to be compensated for. In the view of these findings, the multi-directional approach adopted from the work of Catry (personal communication) was suggested as a possible solution to the incorrect angle repartition of the drag. Unfortunately, we were not able to obtain the positive results when applying this modification in ALADIN CHMI framework.

Although the objectives of the work were not entirely fulfilled, we obtained a more detailed insight into the problem of the envelope suppression and better understanding of the sensitivity and response of the scheme to new tuning as well as to several complementary modifications, which has a great value for the further development.

Bibliography

BOER, G. J., MCFARLANE, N. A., LAPRISE, R., HENDERSON, J. D. AND BLANCHET, J.-P. *The Canadian Climate Center spectral atmospheric General Circulation Model* 22, 397-429, 1984

BOUGEAULT, P. *Sub-grid orography parametrizations.* ECMWF, 2001

CATRY, B. *Effects of moisture and mountains in Numerical Weather Prediction.* 2005

CATRY, B., GELEYN, J.-F., BOUYSSEL, F., CEDILNIK, DEJONGHE, J., DERKOVÁ, M., MLÁDEK, R. *Evolutions of the mountain drag/lift parametrization scheme in ARPEGE/ALADIN. Part II: tunning and validation of the new scheme.* submitted to Q.J.R.M.S. June 2005

GELEYN, J.-F., BOUYSSEL, F., CATRY, B., BEAU, I., BROŽKOVÁ, R. AND DRVAR, D. *Evolutions of the mountain drag/lift parametrization scheme in ARPEGE/ALADIN. Part I: conceptual choices and their justification.* submitted to Q.J.R.M.S. June 2005

GERARD, L. *Subgrid dynamic Processes.* 1999

HOLTON, J. R. *An introduction to dynamical meteorology.* Academic Press Inc., third edition, 1992

LINDZEN, R. S. *Turbulence and stress owning to gravity wave and tidal breakdown.* J. Geophys. Res., 86, 9707-9714, 1981

LOTT, F. *Allevation of Stationary Biases in a GCM through a mountain drag parametrization scheme and a simple represenation of mountain lift forces.* Mon. Wea. Rev., 127, 788-801, 1999

LOTT, F., MILLER, M. J. *A new subgrid-scale orographic drag parametrization:Its formulation and testing.* Q. J. R. Meteorol. Soc., 123, 101-127, 1997

MOBBS, S. D. *The parametrization of sub-grid scale orography.* ECMWF, 1994

OLAFSSON, H. AND BOUGEAULT, P. *The effect of rotation and surface friction on orographic drag.* J. Atmos. Sci., 54, 193-210, 1997

PELTIER, W. R. AND CLARK, T. L. *Critical level reflection and the resonant growth of nonlinear mountain waves.* J. Atm. Sci., 41(21), 3122-3134, 1984

PHILLIPS, D. S. *Analytical surface pressure and drag for linear hydrostatic flow on three-dimensional elliptical mountains.* J. Atmos Sci., 41, 1073-1084, 1984

PIERREHUMBERT, R. T. *Linear results on the barrier effects on the mesoscale mountains.* J. Atmos Sci., 40, 1073-1084, 1983

SCINOCCA, J. F AND MC FARLANE, N. A. *The parametrisation of drag induced by stratified flow over anisotropic orography.* Q. J. R. Meteorol. Soc., 121, 1005-1021, 2000

SIMON, A., HORVÁTH, A., VIVODA, J. *Case study and numerical simulations of the 19 November 2004 severe windstorm in central Europe.*

WALACE, J. M., TIBALDI, S. AND SIMMONS, A. J. *Reduction of systematic forecast errors in the ECMWF model through the introduction of an envelope orography.* Q. J. R. Meteorol. Soc., 129, 1989-2010, 1983

WEBSTER, S., BROWN, A. R., CAMERON, D. R., JONES, C. P. *Improvements to representation of orography in the Met Office Unified Model.* Q. J. R. Meteorol. Soc., 109, 683-717, 2003

Notations

α	mountain shape parameter (tuning constant)
β	portion of the "isolated" lower level flow (tuning constant)
C_d	coefficient for the form drag (tuning constant)
f	Coriolis parameter
f'	Coriolis-like parameter concerning a lift force
F	$= NH/U$, inverse Froude number (or non-dimensional mountain height)
F_c	critical F value (tuning constant)
g	gravitational acceleration
h	standard deviation of the unresolved orography
$\mathcal{H}$	$= Rh$ effective mountain height
$\mathcal{H}_p$	effective mountain height (in pressure coordinates) used in low level averaging
κ	coefficient for the surface stress (tuning constant)
κ'	$= \kappa F/F_c$, quantity replacing κ when $F < F_c$
k	$= 2\pi/\lambda$ horizontal wavenumber
ℓ	Scorer parameter
m	vertical wavenumber
N	Brunt-Väisäla frequency
p	air pressure
R	ratio $\mathcal{H}/h$ (tuning constant)
ρ	air density
S	shape of the mountain (functional volume representation)
T	$= \mathcal{H}F_c/F$, wave-generation depth
$\vec{\tau}$	total surface stress vector
τ_f	form-drag induced surface stress magnitude
τ_{lin}	linear-theory value for the surface stress magnitude
τ_w	wave-drag induced surface stress magnitude
u	zonal wind component
v	meridional wind component
$\vec{v}$	wind vector
w	vertical wind component
Z_b	$= \mathcal{H}(1 - F_c/F)$, blocked flow depth